CHALMERS
UNIVERSITY OF TECHNOLOGY

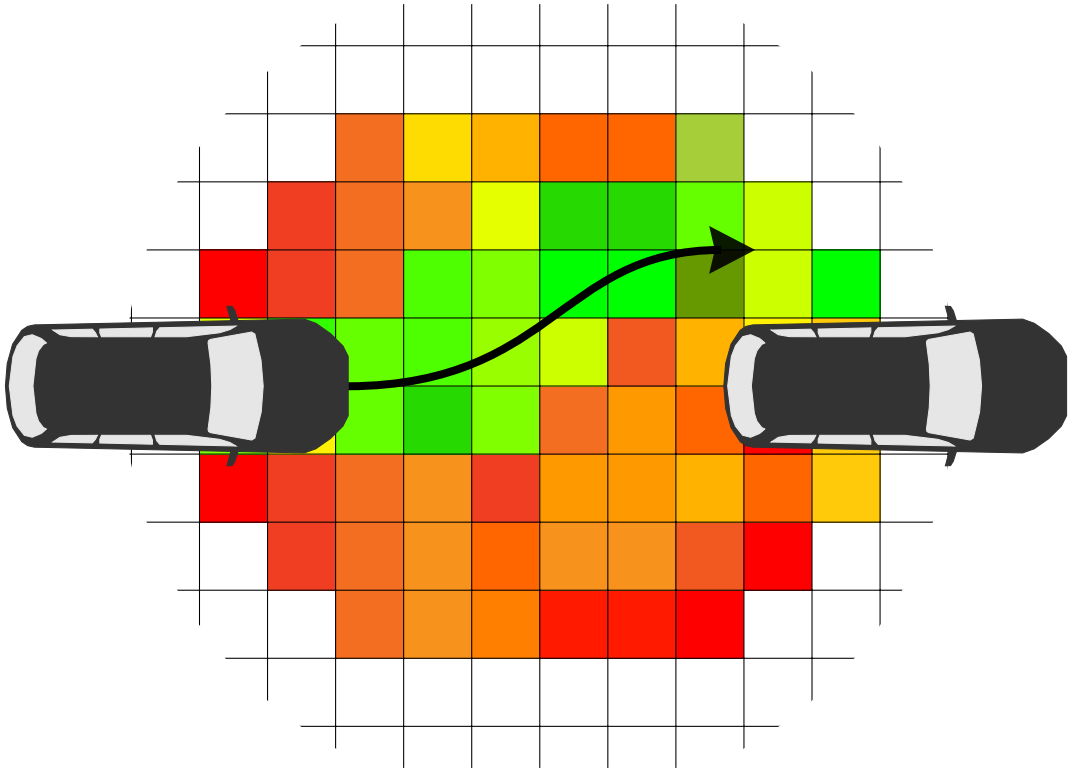

Collision Avoidance by Utilizing Dynamic Road Friction Information

An approach for the usage of road friction information in path planning and motion control algorithms to improve collision avoidance applications

Master's thesis in Master Programme Systems, Control and Mechatronics

JONAS HERZFELD
SANJIV THOTTATHODHI

Department of Electrical Engineering
CHALMERS UNIVERSITY OF TECHNOLOGY
Gothenburg, Sweden 2020

Master's thesis 2020

Collision Avoidance by Utilizing Dynamic Road Friction Information

An approach for the usage of road friction information in path planning and motion control algorithms to improve collision avoidance features

JONAS HERZFELD
SANJIV THOTTATHODHI

CHALMERS
UNIVERSITY OF TECHNOLOGY

Department of Electrical Engineering
Division of Systems and Control
Chalmers University of Technology
Gothenburg, Sweden 2020

Collision Avoidance by Utilizing Dynamic Road Friction Information.
An approach for the usage of road friction information in path planning and motion control algorithms to improve collision avoidance features.
JONAS HERZFELD, SANJIV THOTTATHODHI

Supervisor: Srikar Muppirisetty, Volvo Cars Corporation
Sohini Roychowdhury, Volvo Cars Technology USA
Mats Jonasson, Chalmers University of Technology
Examiner: Jonas Sjöberg, Chalmers University of Technology

Master's Thesis 2020
Department of Electrical Engineering
Division of Systems and Control
Chalmers University of Technology
SE-412 96 Gothenburg
Telephone +46 31 772 1000

Cover: Visualization of varying friction profile and resulting path planning of ego vehicle.

Typeset in LaTeX
Printed by Chalmers Reproservice
Gothenburg, Sweden 2020

Collision Avoidance by Utilizing Dynamic Road Friction Information.
An approach for the usage of road friction information in path planning and motion control algorithms to improve collision avoidance features.
JONAS HERZFELD, SANJIV THOTTATHODHI
Department of Electrical Engineering
Division of Systems and Control
Chalmers University of Technology

Abstract

Slippery road conditions are known to influence the car's ability to brake or steer. Conventional Advanced Driver Assistance Systems (ADAS) such as Autonomous Emergency Braking (AEB) and Autonomous Emergency Steering (AES) systems do not consider road friction at all or assume constant friction in the threat assessment. This is to ensure that the system does not intervene if the driver can still avoid a collision, thereby reducing the number of false positive interventions. Ignoring the varying road friction leads to inefficient operation under slippery road surface conditions. Therefore in this thesis, we present a novel AEB and AES system that exploits friction information ahead of the ego vehicle which is predicted using onboard vehicle sensors as well as cloud services. The proposed algorithms utilize dynamic friction profiles and enable collision prevention by braking or steering.

The AEB system is realized by implementing a simplified vehicle model that enables fast online computations to evaluate the braking distance. Next, the braking sequence is initiated by an anti-lock braking system with slip control. The performance of the proposed algorithm and controller is simulated and evaluated in terms of the braking distance metric that evaluates the relative distance between the ego vehicle and the threat vehicle at standstill. The proposed algorithm achieves an improvement of up to 95.8% for varying friction profiles when compared to braking error obtained assuming constant friction profiles. Furthermore, the proposed algorithm is capable of preventing collisions in all experimental tests while also reducing false interventions, thus making it suitable for designing active safety functionalities.

The AES system is realized in two separate ways, by incorporating the friction as a constraint on a model predictive control (MPC) regulator and by using it to influence the maximum curvature in a curve-based path planner. The performance of the proposed solutions are simulated and evaluated in terms of the distance to the threat vehicle at which a lane change is initiated and if a collision is prevented. It is shown that both approaches prevented collisions in all experimental tests. While the MPC showed the best performance for perfect friction measurements and was able to provide smooth trajectories it lacked robustness against noise on the predicted friction measurements. The path planner based solution provided more conservative results but showed to be more robust against noise on predicted friction measurements.

Keywords: Emergency Braking, Emergency Steering, AEB, AES, ADAS, Road Friction, MPC, Path Planning, Motion Control.

Acknowledgements

We would like to express our gratitude to Professor Jonas Sjöberg who helped us with valuable advice and always found time to discuss problems and solutions with us. Furthermore, we would like to thank Mats Jonasson for his help and availability especially concerning topics of Vehicle Modeling as well as Sohini Roychowdhury for her frequent advice. A special thanks is going to Srikar Muppirisetty from Volvo Cars Corporation for initiating this project and supporting us in every way.

Jonas Herzfeld and Sanjiv Thottathodi, Gothenburg, June 2020

Contents

List of Figures

List of Tables

Acronyms and Nomenclature

Acronyms

ABS Anti-lock Braking System
ADAS Advanced Driver Assistance Systems
AEB Autonomous Emergency Braking
AES Autonomous Emergency Steering
COG Center of gravity
DOF Degrees of freedom
MPC Model Predictive Control
TTC Time To Collision
TTS Time To Steer

Nomenclature

$\dot{x}$	First order derivative of variable x with respect to time
$\ddot{x}$	Second order derivative of variable x with respect to time
$s_{x/y}$	Distance in meter in x- or y-direction
$v_{x/y}$	Velocity in meter per second in x- or y-direction
$a_{x/y}$	Acceleration in meter per second squared in x- or y-direction
$J_{x/y}$	Jerk in meter per second cubic in x- or y-direction
μ	Tire road friction coefficient
δ	Steering input angle in radians
Ψ	Yaw angle in radians
$\dot{\Psi}$	Yaw rate of the vehicle
β	Vehicle slip angle in radians
α	Tire slip angle in radians
σ_x	Tire slip ratio
a	Vehicle front axle distance to COG in meter
b	Vehicle rear axle distance to COG in meter
l	Vehicle wheel base in meter
w	Vehicle width in meter
m	Vehicle mass in kilogram
h	Height of COG in meter
J	Vehicle moment of inertia in kilograms times meter squared
$F_{x,F/R}$	Vehicle longitudinal force front or rear wheels in Newton
$F_{y,F/R}$	Vehicle lateral force front or rear wheels in Newton
F_z	Total normal force in Newton
C_α	Cornering Stiffness
C_σ	Longitudinal Stiffness
f_r	Rolling resistance coefficient
κ	Binary time delay coefficient
p	Tuning gain for lateral force compensation
K_{Lat}	Lateral force compensation
L	Initial distance of ego vehicle and threat vehicle in test scenario in meter
K_L^{max}	Maximum curvature left lane
K_R^{max}	Maximum curvature right lane
K_{sys}^{max}	Maximum curvature of corresponding to maximum lateral acceleration
N	Model predictive control prediction horizon length
σ	Standard deviation

1
Introduction

1.1 Motivation

This thesis investigates the influence of road friction information in Advanced Driver Assistance Systems (ADAS) such as Autonomous Emergency Braking (AEB) and Autonomous Emergency Steering (AES) applications. Conventional AEB systems are designed to minimize the number of false interventions of the system i.e the system should not intervene if the driver can handle the situation. Therefore, the AEB system is developed by estimating the shortest braking distance under high road friction conditions. This leads to a reduction in the number of false interventions from the system, though also yields the threat of overestimating the real braking performance under low road friction conditions.

The road surface friction information is not always constant and plays an important role in active safety development. For instance, a change in the road profile or the weather conditions will impact the braking capabilities of the vehicle and influence the performance of active safety systems. Studies have shown the great impact road conditions can have on the occurrence of collisions. For example, the work in [1] analyses accidents on U.S. roads from 1995 to 2005 and states that 24% of the collisions are weather-related, 99% of which occur on slick pavement. Furthermore [2] indicates that the risk of an accident in rainy conditions is two to three times greater than in dry conditions.

To ensure the safe operation of the autonomous vehicle in all weather conditions, road awareness is key. With the technology and sensors available today it is possible to predict the road conditions and studies have been carried in [3] which describe the use of vision sensors and deep learning models to predict the road surface coefficient. This thesis assumes access to road surface friction information and focuses on exploiting the friction information to develop a novel vehicle motion control architecture and path planning algorithms to improve the performances of active safety systems.

1.2 Overview

The objective of the thesis is to develop novel vehicle motion control and path planning algorithms that effectively utilize the predicted friction information in collision avoidance applications. With these new algorithms, it shall be possible to prevent or

mitigate collisions for varying, non-uniform friction as well as prevent false-positive interventions. An accurate vehicle model shall be designed to effectively capture the influence of friction on the vehicle dynamics. They shall be compared with conventional active safety systems that do not take predicted non-uniform friction information into account to trigger an intervention with common evaluation metrics such as the last point to start braking/steering.

Two critical scenarios are investigated, collision avoidance by emergency braking and collision avoidance by emergency steering. The emergency braking scenario assumes a stationary threat vehicle in the path of the ego vehicle and the active safety system triggers a braking maneuver to prevent a collision. The system takes the varying friction conditions ahead of the ego vehicle into account like for example an ice patch on the braking path. Figure 1.1 illustrates the problem.

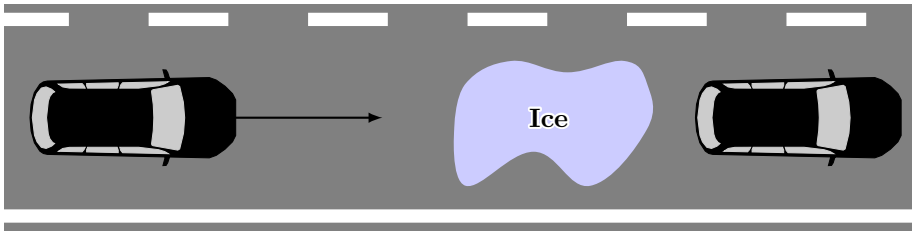

Figure 1.1: Rear-end emergency braking scenario with known road friction profile.

An alternative to prevent a rear-end collision is to perform an emergency steering maneuver and change the lane when the threat vehicle in lane appears to be slowing down or stopped. The intention is that the developed algorithm should calculate an optimal lane change path based on the friction, that the vehicle needs to follow in order to prevent a collision based on steering. This is aimed to be achieved by two methods, one that utilizes a model predictive control (MPC) regulator which performs optimal path planning inherently and the alternative is to modify existing path planning algorithms to incorporate friction information in them to calculate the desired path.

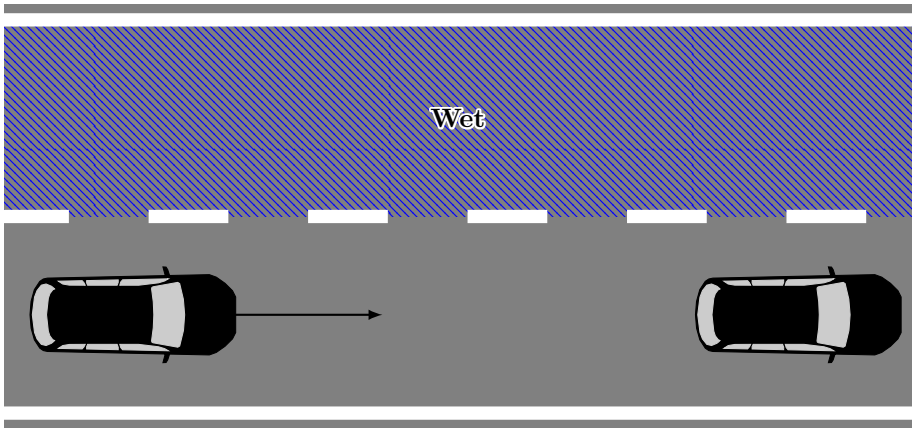

Figure 1.2: Lane change emergency steering scenario with known road friction profile.

1.3 Evaluation Metrics

The performance measure for the emergency braking scenario used in this thesis is the error in braking distance calculation, i.e., how far from the threat the ego vehicle comes to a standstill. Positive values indicate stopping in front of the stationary vehicle, while negative values indicate a collision as the vehicle comes to hold behind the stationary vehicle. The measure is chosen as a value of zero indicates an optimal triggering of the brake maneuver and utilization of the road friction. A high positive or negative value on the other side indicate under-/overestimation of road friction and possible false-positive interventions.

As a baseline, the developed algorithm shall be compared to the performance achieved without online friction information i.e. assuming a constant value. Two road surface conditions have been assumed as constant conditions, dry concrete and snow. The baseline brake distance for these cases is determined based on the tool given in [4]. It is expected that assuming a braking distance based on dry concrete will lead to collisions in all test cases as the braking performance is overestimated. In contrast, assuming constant snowy road conditions leads to rather conservative results and potential false positive AEB deployment. Figure 1.3 illustrates the evaluation metric for the proposed AEB in comparison to the baseline systems.

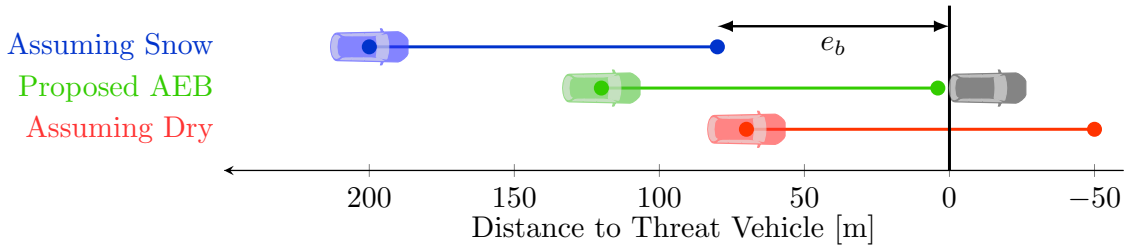

Figure 1.3: Example of the brake distance from initiation to standstill for the proposed AEB and the baseline systems. Example of evaluation metric e_b for the case of assuming snow.

In the emergency steering scenario, a similar metric is chosen. The goal is to utilize the road friction to the maximum amount such that the lane change is performed in the last moment while keeping the vehicle stable. Therefore the chosen measure is the distance to the threat vehicle at which the lane change is initiated. As baseline, a simple polynomial curve-based path is generated based on the assumption of constant friction. The baseline is explained in more detail in Section 2.3.

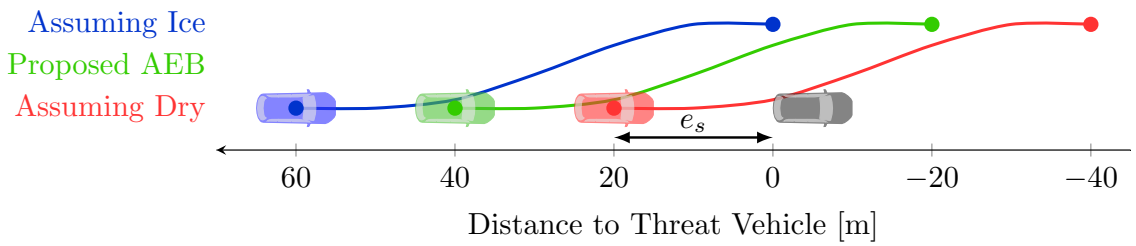

Figure 1.4: Example of lane change maneuver from initiation to completion for the proposed AES and the baseline systems. Example of evaluation metric e_s for the case of assuming dry roads.

1.4 Scientific Contribution

The main scientific contributions from this thesis are:

Autonomous Emergency Braking

- A novel brake distance algorithm is developed that utilizes varying friction information in its estimation of required braking distance.
- A simple 4-wheel vehicle model with approximations and modifications is modeled to ensure accurate predictions in braking distance while retaining computational speed.
- The performance of the proposed algorithm is validated using a high accuracy IPG CarMaker model [5].
- An improvement in the estimation of brake distance up to 95.8% of the proposed algorithm is achieved for dynamic friction profiles in comparison to a system that assumes constant friction profiles.

Autonomous Emergency Steering

- An AES algorithm using Model Predictive Control based regulator which takes varying friction as part of the constraint set on lateral forces is developed.
- A novel AES algorithm using a path planning framework is proposed that utilizes varying friction information in a path to determine the last point to steer.
- The two proposed AES algorithms are validated using a high accuracy IPG CarMaker model [5].
- Results achieved from the developed algorithms show successful collision avoidance for dynamic friction information and improvement of path prediction quality in comparison to the assumption of constant friction.

2
Mathematical Models

This section will explain the most important concepts and theories necessary to follow the outline of the thesis. In particular, the methods used to predict the road surface conditions will be explained as well as the basics of vehicle modeling which are fundamental for path planning and motion control applications. Additionally the baseline system for the AES evaluation will be introduced.

2.1 Road Surface Friction Estimation

The relation between road surface friction and the forces acting on the vehicle tires is introduced in this chapter. Furthermore, the different approaches used to estimate the road surface friction under the tire or ahead of the vehicle are presented.

2.1.1 Definition of Road Friction

The road friction coefficient μ is defined as the maximum normalized traction force which can be generated at the tire

$$\mu = \frac{\sqrt{F_x^2 - F_y^2}}{F_z}, \tag{2.1}$$

where F_x, F_y are the longitudinal and lateral forces acting on the tire and F_z is the normal force [6, pp. 433]. The value of μ depends on the road condition which means that for example on dry concrete surfaces μ can reach values of 1 while for icy surfaces the value of μ tends to be below 0.1. This has a major impact on the performance of active safety and vehicle automation applications as it limits the amount of force which can be applied at the tire.

2.1.2 Friction estimation under tire

There is a variety of friction estimation algorithms used in practice that are applied to provide input for example to traction or anti-lock braking system (ABS) controllers. These estimators can be roughly summarized in two categories:

1. Experiment-based,
2. Model-based.

Experiment-based approaches try to estimate the road friction by analyzing sensor data of friction-correlated parameters. Such sensors include for example infrared

cameras directed at the road surface which give information about the road condition based on the wavelength of the reflected light, acoustic sensors can be used to estimate the road condition and type from the noise generated by the tire or tread sensors give an indication on the deformation of the tire based on the road conditions. With this sensor input, it was shown that an accurate estimation of the road surface is possible though the experiment-based approaches cannot often repeatedly achieve similar results. As the approach is highly fitted to a certain test and car setup, a change in the parameters (e.g. tire pressure, tire temperature, etc.) has a high influence on the accuracy of the results [7].

The second category of friction estimation algorithms is model-based algorithms. Here models of the wheel and vehicle dynamics, slip dynamics, or the tire model are used to approximate the road friction coefficient. Vehicle model-based approaches make use of simplified equations of vehicle dynamics together with state estimator algorithms like Kalman Filters to approximate the friction. Slip-based models make use of a relation between the slope of the friction curve for low slip values and the maximum achievable friction value at saturation of the tire. Tire model-based approaches apply a detailed tire model like the Magic formula, Brush model, etc. to estimate the friction from tire forces and slip [7].

The proposed methods are well proven in several applications and give valuable input for safety functions like traction and ABS control. A limitation of the approaches though is that they can only give accurate estimates of the friction values under or behind the ego vehicle as they rely on sensor measurements at the tire. To make more sophisticated active safety functions like AEB or AES robust against adverse weather and changing road conditions an accurate prediction of friction values ahead of the vehicle is necessary.

2.1.3 Friction prediction ahead of vehicle

Research has been carried out to predict the road friction values ahead of the vehicle based on machine learning models. The method described in [3] takes advantage of the onboard vehicle sensors of the ego vehicle to estimate the road friction profile ahead. The data from the sensor is processed into road patches and using deep neural networks it is shown that it is possible to classify the road surface conditions into three classes: dry, wet, and icy. A rule-based model is then utilized to estimate the road friction coefficient with an accuracy of 89.3%. The results from [3] show that it is possible to perform real-time estimation of road surface conditions ahead of the vehicle. This new information can be exploited in redesigning current active safety systems to improve their performance and operation domain. Additionally, there are existing services that provide road friction information as a cloud-based service. Predictions are made based on weather forecasts and can be combined with swarm intelligence-based algorithms. Cars can send the estimated friction coefficients calculated under the vehicle tires with high accuracy to a cloud service and provide it to following vehicles [8].

In this thesis it is assumed that a road friction coefficient prediction ahead of the ego road section is provided by a sensor based on machine learning or cloud-based services. The varying friction ahead is predicted as $\tilde{\mu}$ with mean and standard deviation in a grid with cell size Δs (see Figure 2.1). Friction values may vary between 0.1 (icy road patches) and 1 (dry concrete).

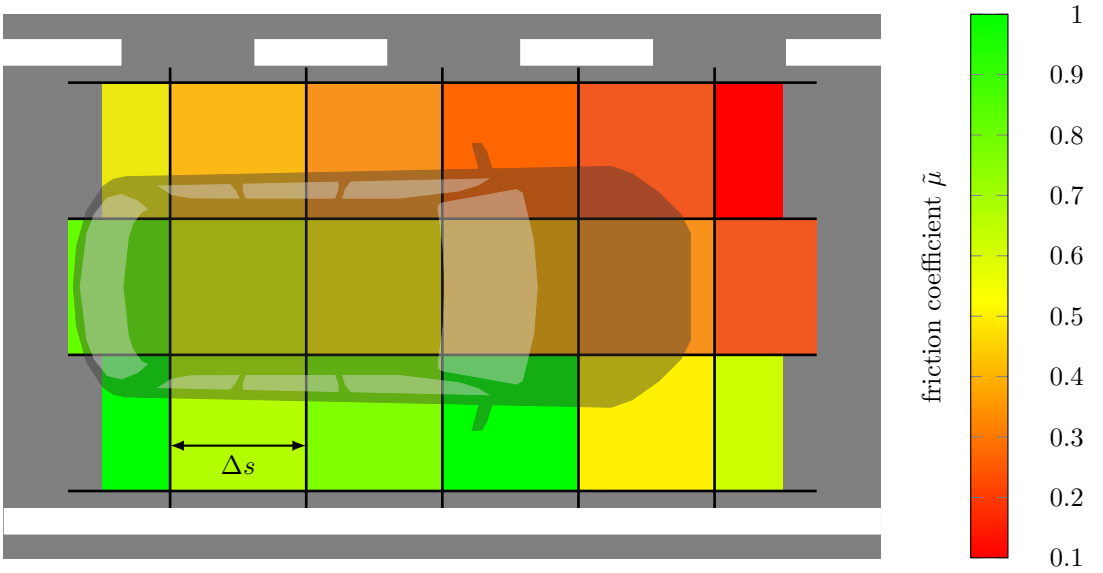

Figure 2.1: Definition of $\tilde{\mu}$-grid on road

2.2 Vehicle Modelling

This section introduces the concept of vehicle modeling. The creation of realistic models to study vehicle behavior is essential in various disciplines of mechanical and mechatronic engineering and is a branch of vehicle dynamics. It is the basis for the development of many vehicle components and safety functions as the models can be used to accurately simulate and predict the vehicle behavior [9, pp. 1].

2.2.1 Point-Mass Model

The point-mass model is a simple vehicle model that reduces the vehicle to a particle which is only bounded by the acceleration that can be applied to it [10]. A typical state space representation of a point-mass vehicle model in 2D is

$$\begin{bmatrix} \dot{s}_x \\ \dot{s}_y \\ \ddot{s}_x \\ \ddot{s}_y \end{bmatrix} = \begin{bmatrix} 0 & 0 & 1 & 0 \\ 0 & 0 & 0 & 1 \\ 0 & 0 & 0 & 0 \\ 0 & 0 & 0 & 0 \end{bmatrix} \begin{bmatrix} s_x \\ s_y \\ \dot{s}_x \\ \dot{s}_y \end{bmatrix} + \begin{bmatrix} 0 & 0 \\ 0 & 0 \\ 1 & 0 \\ 0 & 1 \end{bmatrix} \begin{bmatrix} \ddot{s}_x \\ \ddot{s}_y \end{bmatrix} \tag{2.2}$$

with $\dot{s}_x = v_x$, $\dot{s}_y = v_y$ and $\ddot{s}_x = a_x$, $\ddot{s}_y = a_y$ subject to $\sqrt{a_x^2 + a_y^2} \leq a^{max}$. Therefore, the forces applied to the point-mass can be limited by a^{max}, the model ignores though that the point-mass has an orientation. This model is used in many applications

concerning motion estimation, planning and control due to its simplicity. In [11] a point mass model is used in path planning for a car in a highway scenario and it was shown that a 4-wheel model was able to accurately follow the path generated by the point mass model. By discretizing the continuous model given in (2.2) it becomes

$$\begin{bmatrix} s_x(k+1) \\ s_y(k+1) \\ v_x(k+1) \\ v_x(k+1) \end{bmatrix} = \begin{bmatrix} 1 & 0 & \Delta t & 0 \\ 0 & 1 & 0 & \Delta t \\ 0 & 0 & 1 & 0 \\ 0 & 0 & 0 & 1 \end{bmatrix} \begin{bmatrix} s_x(k) \\ s_y(k) \\ v_x(k) \\ v_y(k) \end{bmatrix} + \begin{bmatrix} \frac{1}{2}\Delta t^2 & 0 \\ 0 & \frac{1}{2}\Delta t^2 \\ \Delta t & 0 \\ 0 & \Delta t \end{bmatrix} \begin{bmatrix} a_x(k) \\ a_y(k) \end{bmatrix}, \tag{2.3}$$

where Δt is equal to the sampling time used to discretize the model.

2.2.2 Bicycle Model

For a more accurate description of the vehicle movement, a commonly used model is the bicycle model. The name originates from the fact that the front and rear wheels of the car respectively are combined into a single wheel per axis and therefore the model representation looks similar to that of a bicycle. The free-body diagram and the respective forces and moments acting on the model is shown in Figure 2.2.

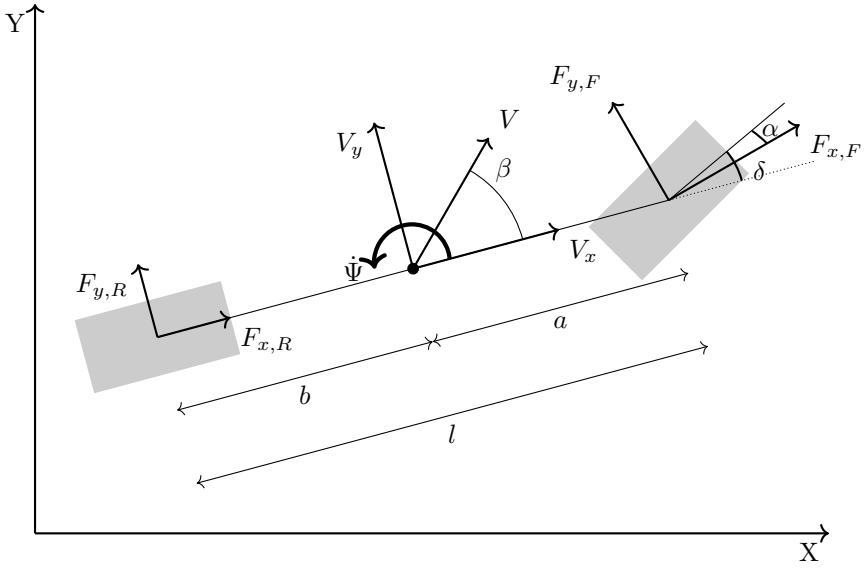

Figure 2.2: Bicycle Model - Free body diagram

2.2.2.1 Linear Bicycle Model for Lateral Motion

The linear bicycle model has 2 degrees of freedom the lateral dynamics and yaw stability. The linear model is usually used when studying the lateral dynamics of the vehicle and longitudinal motion is not of prime importance. The longitudinal velocity is assumed to be constant and the longitudinal forces are neglected in the analysis. The longitudinal and lateral acceleration in the inertial frame are given by

$$\begin{aligned} a_x &= \dot{v}_x - v_y\dot{\Psi} \\ a_y &= \dot{v}_y + v_x\dot{\Psi}. \end{aligned} \tag{2.4}$$

By neglecting roll and pitch motion the vehicle forces can be written as

$$\begin{aligned} \dot{v}_y &= -v_x\dot{\Psi} + \frac{F_{y,R} + F_{y,F}\cos(\delta) - F_{x,F}\sin(\delta)}{m} \\ \ddot{\Psi} &= \frac{aF_{x,F}\sin(\delta) + aF_{y,F}\cos(\delta) - bF_{y,R}}{J} \end{aligned} \tag{2.5}$$

where δ is the steering input angle, Ψ is the yaw angle, and J is the moment of inertia of the vehicle. The respective longitudinal and lateral tire forces are approximated with a linear tire model which is given by

$$\begin{aligned} F_{x,i} &= C_{\sigma i}\sigma_{xi} \quad i \in (F,R) \\ F_{y,i} &= C_{\alpha i}\alpha_i \quad i \in (F,R) \\ \sigma_{xi} &= \frac{r_{eff}\omega - v_x}{\max(v_x, r_{eff}\omega)} \\ \alpha_F &= \delta - \tan^{-1}(\frac{v_y + a\dot{\Psi}}{v_x}) \\ \alpha_R &= -\tan^{-1}(\frac{v_y - b\dot{\Psi}}{v_x}) \end{aligned} \tag{2.6}$$

where $C_{\sigma i}$, $C_{\alpha i}$ are the longitudinal stiffness, cornering stiffness coefficients and σ_{xi} , α_i are the longitudinal slip ratio and side slip angle respectively. The effective tire radius is depicted as r_{eff} and the wheel speed as ω. The linear bicycle model can be written in state space form

$$\begin{bmatrix} \dot{v}_y \\ \ddot{\Psi} \end{bmatrix} = \begin{bmatrix} -\frac{C_{\alpha F}+C_{\alpha R}}{mv_x} & \frac{-aC_{\alpha F}+bC_{\alpha R}}{mv_x} - v_x \\ -\frac{aC_{\alpha F}-bC_{\alpha R}}{J} & -\frac{a^2C_{\alpha F}+b^2C_{\alpha R}}{J} \end{bmatrix} \begin{bmatrix} v_y \\ \dot{\Psi}(k) \end{bmatrix} + \begin{bmatrix} \frac{C_{\alpha F}}{m} \\ \frac{aC_{\alpha F}}{J} \end{bmatrix} \begin{bmatrix} \delta \end{bmatrix}. \tag{2.7}$$

As stated earlier the lateral dynamics can be expressed in a linear model because the longitudinal velocity v_x is considered constant. To model the longitudinal dynamics a nonlinear model or a linear parameter varying model has to be used.

2.2.2.2 Non-Linear Bicycle Model for combined Lateral and Longitudinal Motion

To enable efficient longitudinal and lateral control, the longitudinal dynamics of the vehicle have to be modeled accurately. By introducing the longitudinal force components into the force balance equations we get

$$\begin{aligned} ma_x &= F_{x,R} + F_{x,F}\cos(\delta) - F_{y,F}\sin(\delta) \\ ma_y &= F_{y,R} + F_{y,F}\cos(\delta) + F_{x,F}\sin(\delta) \\ J\ddot{\Psi} &= aF_{x,F}\sin(\delta) + aF_{y,F}\cos(\delta) - bF_{y,R} \end{aligned} \tag{2.8}$$

The lateral and longitudinal acceleration in inertial frame are given as in (2.4). Based on (2.4) and (2.8) the motion equation for the bicycle model with 3 degrees

of freedom can be expressed as

$$\begin{aligned} \dot{v}_x &= v_y\dot{\Psi} + \frac{F_{x,R} + F_{x,F}\cos(\delta) - F_{y,F}\sin(\delta)}{m} \\ \dot{v}_y &= -v_x\dot{\Psi} + \frac{F_{y,R} + F_{y,F}\cos(\delta) - F_{x,F}\sin(\delta)}{m} \\ \ddot{\Psi} &= \frac{aF_{x,F}\sin(\delta) + aF_{y,F}\cos(\delta) - bF_{y,R}}{J} \end{aligned} \tag{2.9}$$

The forces F_x and F_y depend on the tire model (see Section 2.2.4) and are bounded by the normal force and the friction value at each tire as $\sqrt{F_x^2 + F_y^2} \leq \mu F_z$. This can also be described as circle of forces (Kamm's circle) [9, p. 167] (see Figure 2.3).

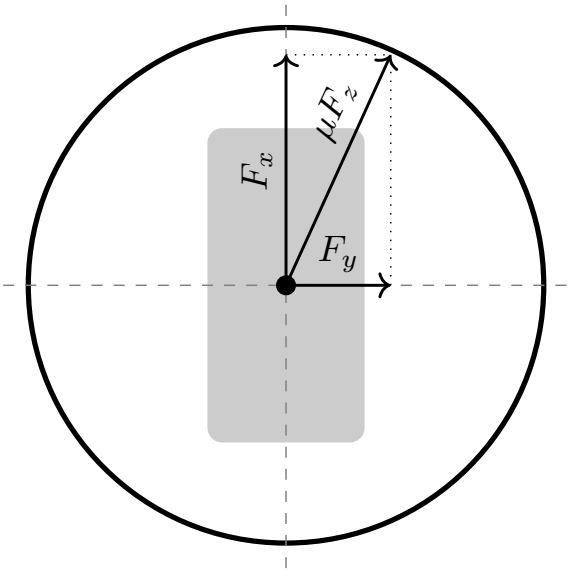

Figure 2.3: Circle of forces at a tire limiting the maximum lateral and longitudinal forces

The static normal forces $F_{z,i}^{stat}$ for each tire in the bicycle model $i \in \{F, R\}$ are calculated based on the location of the center of gravity in the vehicle frame.

$$\begin{aligned} F_{z,F}^{stat} &= \frac{mgb}{l} \\ F_{z,R}^{stat} &= \frac{mga}{l} \end{aligned} \tag{2.10}$$

In order to accurately capture the forces acting on the vehicle during acceleration and deceleration the effects of load transfer have to be taken into account. During longitudinal acceleration, the normal forces $F_{z,i}$ acting on the front tires are reduced while the normal forces on the rear tires increase. This shift of the load and therefore the change in normal forces can approximately be modeled as a function of longitudinal acceleration on the vehicle frame [12]. The force induced due to load transfer is calculated as

$$\Delta F_{long} = \frac{ma_x h}{l}. \tag{2.11}$$

This results in an updated normal force which consists of the static normal force and the change due to load transfer

$$\begin{aligned} F_{z,F} &= F_{z,F}^{stat} - \Delta F_{long} \\ F_{z,R} &= F_{z,R}^{stat} + \Delta F_{long}. \end{aligned} \tag{2.12}$$

Even though the bicycle combines both tires on an axle to one, also the lateral load transfer can be modeled for each tire which can be useful for certain applications.

2.2.3 4-Wheel Model

In comparison to the bicycle model, the 4-Wheel model does not simplify the front tires and rear tires respectively to a single tire per axis. This adds complexity to the model as the lateral and longitudinal forces on each tire are calculated and tracked. It also allows a more realistic simulation of the vehicle behavior, especially concerning the lateral motion when different forces are applied to the left and the right side of the vehicle. This can give important insights concerning the influence of laterally differing friction values and the impact on the emergency braking and steering applications.

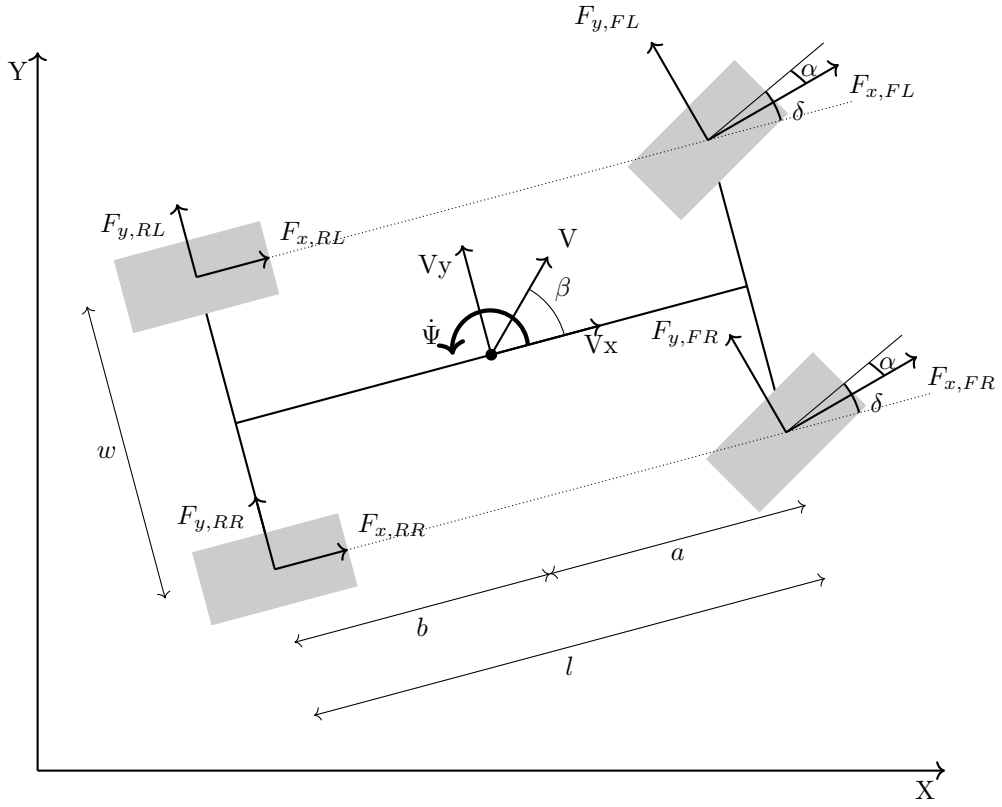

Figure 2.4: 4-Wheel vehicle model with force definitions.

With four tires the force balance equation is given by

$$\begin{aligned} ma_x &= F_{x,RL} + F_{x,RR} + (F_{x,FL} + F_{x,FR})\cos(\delta) - (F_{y,FL} + F_{y,FR})\sin(\delta) \\ ma_y &= F_{y,RL} + F_{y,RR} + (F_{y,FL} + F_{y,FR})\cos(\delta) - (F_{x,FL} + F_{x,FR})\sin(\delta). \end{aligned} \tag{2.13}$$

The torque balance equation is equally adjusted to take the different forces at each wheel into account.

$$J\ddot{\Psi} = \left\{ \begin{array}{r} a(\sin(\delta)(F_{x,FL} + F_{x,FR}) + \cos(\delta)(F_{y,FL} + F_{y,FL})) \\ -b(F_{y,RL} + F_{y,RR}) \\ +\frac{w}{2}(\cos(\delta)(F_{x,FR} - F_{x,FL}) + \sin(\delta)(F_{y,FL} - F_{y,FR}) \\ +\frac{w}{2}(F_{x,RR} - F_{x,RL}) \end{array} \right\} \tag{2.14}$$

With these 3 degrees of freedom (DoF) 4-Wheel model it is possible to simulate the vehicle dynamics in x,y-dimension, and yaw motion. The dynamics along the z-axis as well as roll and pitch are neglected. As the accurate usage of the available friction is highly dependent on the existing normal forces at each tire $F_{z,i}$, the load transfer shall be taken into account even without modeling of roll and pitch motion. The method introduced in Section 2.2.2.2 shall be applied to simulate a load transfer based on the longitudinal and lateral acceleration. For this, the lateral load transfer is approximated as

$$\Delta F_{lat} = \frac{m a_x h}{w}. \tag{2.15}$$

resulting in the following normal force calculation for each tire

$$\begin{aligned} F_{z,FL} &= F_{z,FL}^{stat} - \Delta F_{long} - \Delta F_{lat} \\ F_{z,FR} &= F_{z,FR}^{stat} + \Delta F_{long} + \Delta F_{lat} \\ F_{z,RL} &= F_{z,RL}^{stat} + \Delta F_{long} - \Delta F_{lat} \\ F_{z,RR} &= F_{z,RR}^{stat} + \Delta F_{long} + \Delta F_{lat} \end{aligned} \tag{2.16}$$

2.2.4 Tire Models

Tire models estimate the forces acting on the tire and therefore play a key role in the accuracy of the whole vehicle model. When the tire model is not capturing the forces acting on the tire correctly this directly translates into an error in the vehicle motion estimation. The longitudinal tire force F_x can be depicted as a function of the longitudinal slip ratio σ_x and the lateral tire forces F_y as a function of the slip angle α. Figure 2.5 shows the longitudinal and lateral tire forces as a function of slip ratio and slip angle respectively.

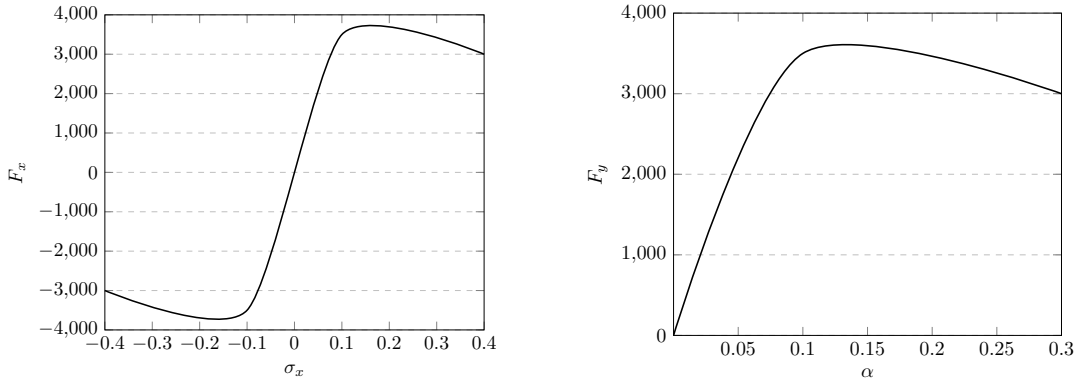

(a) Longitudinal force F_x as a function of the slip ratio σ_x

(b) Lateral force F_y as a function of the slip angle α

Figure 2.5: Tire force as a function of side slip angle and slip ratio

From the figure, it can be observed that the relation between tire forces and slip are nonlinear in nature. Therefore even though linear tire models are able to capture the forces decently for low values of σ_x and α, a nonlinear tire model is required for the accurate approximation of tire forces in all cases. There are numerous tire models approximating the forces experienced by the tires such as the Magic Tire formula, Dugoff's model or the Brush model. In this project, the forces experienced by the tire are modeled as an approximation based on the tangents hyperbolicus (tanh) function.

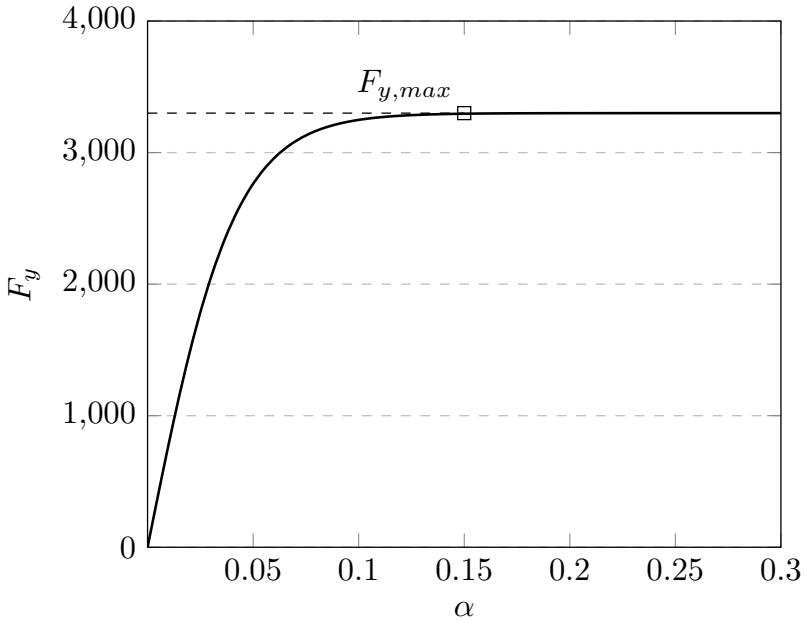

Figure 2.6: Approximation of lateral forces based on the tanh model.

Figure 2.6 illustrates that the tanh approximation gives a good approximation of the tire forces up until the maximum permissible force and saturates past this point. Semi-empirical models like the Magic Tire formula or Dugoff's model are highly dependent on accurate knowledge of specific tire parameters [13]. The tanh approximation on the other hand proposes a very generic solution to the estimation of tire forces with a minimum number of parameters that is computationally easy and requires little adjustment for different tires. The forces are approximated as

$$\begin{aligned} F_{y,i} &= \mu_i F_{z,i} \tanh\left(\frac{C\alpha_i}{\mu_i F_{z,i}}\right) \\ F_{x,i} &= \mu_i F_{z,i} \tanh\left(\frac{C\sigma_{x,i}}{\mu_i F_{z,i}}\right) \end{aligned} \tag{2.17}$$

with $i \in \{FL, FR, RL, RR\}$.

2.3 Baseline for Emergency Steering

As introduced in Section 1.3 a baseline is needed to benchmark the developed emergency steering application with a solution that assumes constant friction. This section provides a brief summary of the algorithm used to benchmark the developed AES system. Assuming constant friction values two simple polynomial paths are created one based on the dry concrete road surface and one based on the constant icy road surface. The technique used to generate the polynomial paths is based on [14], in which the authors discuss polynomial-based path planning, with constraints defined on the maximum lateral acceleration and maximum jerk.

In the proposed lane change path planning algorithm in [14], the authors define the lateral acceleration profile of the vehicle during lane change by using a third order polynomial as:

$$a_y(t) = c_3 t^3 + c_2 t^2 + c_1 t + c_0 \tag{2.18}$$

Where, $c_i, i \in \{0, 1, 2, 3\}$ are the polynomial coefficients, and t is the time variable. Using maximum acceleration limits defined by the approximation $a_y^{max} = \mu g$, the baseline lane change path is generated while limiting the value of a_y^{max} to a maximum of $7\frac{m}{s^2}$. By defining boundary conditions on acceleration profile and jerk as shown in Figure 2.7, the planned acceleration profile of the lane change trajectory is expressed as:

$$a_y(t) = \begin{cases} \frac{a_y^{max}}{T_1}\left(\frac{-2t^3}{T_1^2} + \frac{3t^2}{T_1}\right) & (0 \le t \le T_1) \\ a_y^{max} & (T_1 \le t \le T_2) \\ a_y^{max} - \frac{a_y^{max}}{T_1}\left(\frac{-2(t-T_1-T_2)^3}{T_1^2} + \frac{3(t-T_1-T_2)^2}{T_1}\right) & (T_1 + T_2 \le t \le 2T_1 + T_2) \end{cases} \tag{2.19}$$

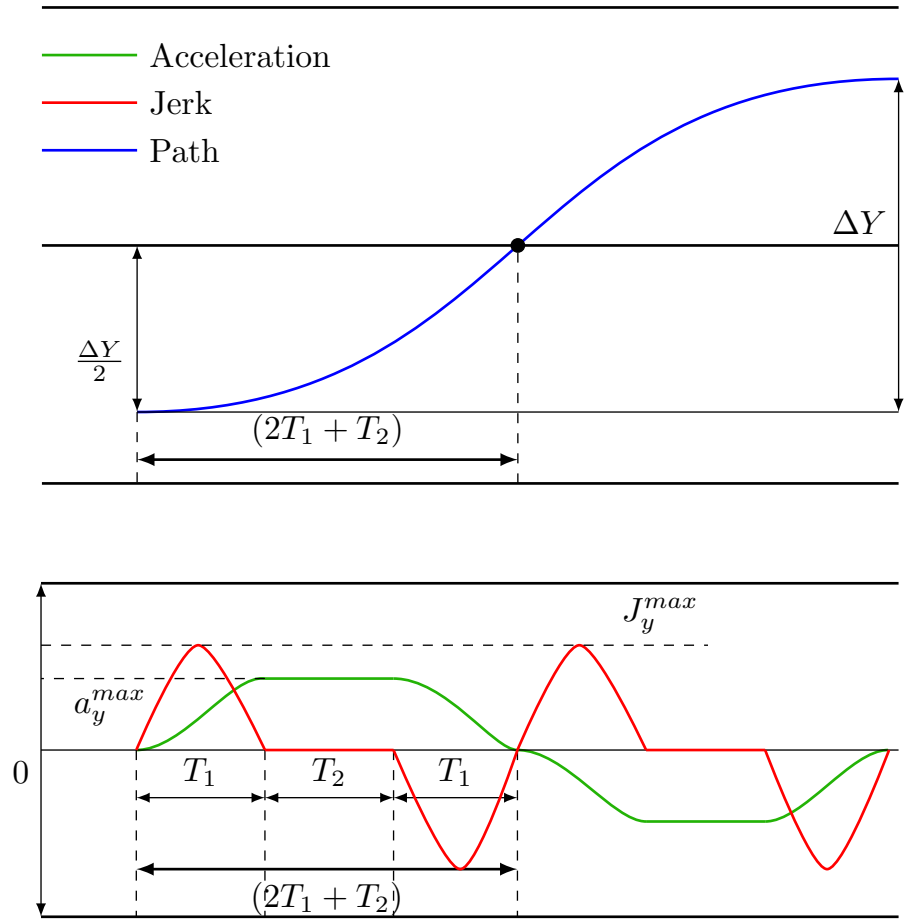

Figure 2.7: Lane change path planned for Baseline

Here, T_1 is the time period during which the the acceleration profile reaches the maximum value from zero and vice versa and is calculated as

$$T_1 = \frac{3a_y^{max}}{2J_y^{max}}, \tag{2.20}$$

where $J_y^{max} \leq 8g$ is the upper bound on maximum value of jerk restrain. Time period T_2 is then obtained by solving equation

$$\frac{\Delta Y}{2} = a_y^{max}(T_1^2 + \frac{3}{2}T_1T_2 + \frac{1}{2}T_2^2). \tag{2.21}$$

The resulting acceleration profile is integrated to obtain the velocity and displacement of the resulting path. The last point to initiate the lane change maneuver is then calculated based on time to collision (TTC) and the predefined threshold set on last time to steer. The last time to steer (TTS) is computed as

$$\text{TTS} = \sqrt{\frac{2 * w}{\mu g}} + \epsilon, \tag{2.22}$$

where w is the minimum lateral safety width required to avoid a collision with the target, g gravity constant, μ road surface friction coefficient and ϵ is a time delay

of 250ms added to compensate for actuator delays in steering input. The time to collision is computed as

$$TTC = \frac{\Delta s}{\Delta v}, \tag{2.23}$$

where Δs is the relative distance to the threat vehicle and Δv is the relative velocity. Once the TTC is lower than the set threshold on TTS, the emergency lane change maneuver is initiated.

3

Autonomous Emergency Braking

In this chapter, we describe the AEB system architecture, the different components in the system architecture and the detailed overview of the developed AEB algorithm that utilizes information about varying friction in decision making.

3.1 Related Work

Conventional ADAS features assume a constant value of road surface friction ahead of the vehicle and compute the threat assessment metrics such as time to collision (TTC) and required safety distance based on the vehicle's deceleration capabilities and tire characteristics. The work in [15] presents an adaptive AEB algorithm that performs a real-time estimation of the road friction coefficient, recomputes the TTC, and adjusts the AEB trigger functionality accordingly. An approach for front collision warning, combining the required braking distance and TTC, computed based on the current road surface friction and vehicle parameters is proposed in [16]. This braking distance is then evaluated against the system limits under low and high friction situations before a warning is sent out. The work in [17] proposes an AEB system that estimates the friction based on the forces acting on the tire and adjusts the TTC accordingly. Further, the method in [18] determines the minimum braking distance based on the current value of friction and road slope. Although these developed algorithms consider the road surface friction, they all assume a constant value of road surface friction in its estimation of required braking distance. The system proposed in the following sections shall be able to prevent collisions for a large variety of road surface conditions by factoring laterally and longitudinally dynamic road friction information into the AEB algorithms.

3.2 AEB Architecture

In the emergency braking scenario, the foremost goal is to brake the ego vehicle down to a velocity smaller or equal than the velocity of a threat vehicle in the ego lane before a collision occurs. Figure 3.1 shows a block diagram of the AEB architecture.

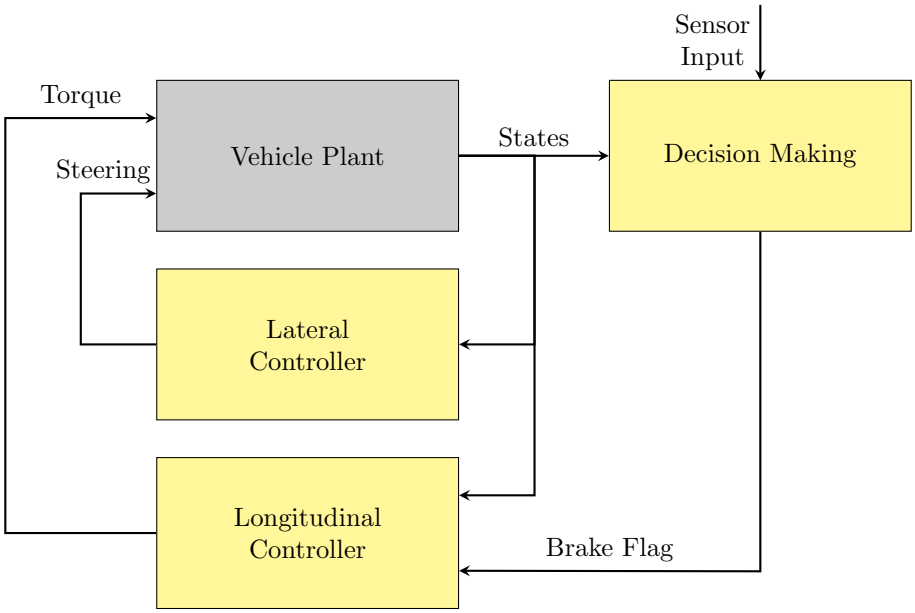

Figure 3.1: System architecture for AEB

The AEB system mainly consists of:

- **Longitudinal Controller** - To apply maximum braking torque to the wheels when AEB is triggered (more details in Section 3.2.1).
- **Lateral Controller** - To ensure the vehicle is staying in lane during the braking sequence (more details in Section 3.2.2).
- **Decision Making Block** - To evaluate the detected threat and provide the controller with the time to initiate braking. (more details Section 3.3)

3.2.1 Longitudinal Controller

To stop the ego vehicle as fast as possible given a road friction profile ahead, the longitudinal control of the vehicle is reduced to the application of maximum available brake torque to the four wheels. Assuming an ideal case of $F_y \approx 0$ the total longitudinal braking force that can be applied is approximately $F_x = \mu F_z$. The longitudinal braking force is a function of the slip ratio and is shown in Figure 3.2. The slip ratio is defined as the ratio between the vehicle speed and the wheel speed. The red region in the figure indicates the slip ratio for which the tire becomes saturated, meaning that the wheel is sliding. This nonlinear region of the tire shall be avoided as it can lead to wheel locking and complete loss of control. For scenarios with low lateral dynamics and high friction values, the approximation of $F_x = \mu F_z$ can give good results in braking down the vehicle without locking the wheels, i.e. applying more force than the circle of forces allows. In the event of considerable lateral dynamics though, applying the maximum force as brake force will lead to an increase of the absolute slip ratio σ_x as the total force exceeds the limit given by μF_z. A slip ratio of -1 indicates that the wheel speed is zero and therefore the wheels are locked while the vehicle speed is still non-zero. Too high absolute slip ratios reduce the amount of longitudinal force that is applied at the wheel as Figure 3.2 shows and for locked wheels even make the vehicle uncontrollable as steering

inputs will not lead to a change in direction anymore.

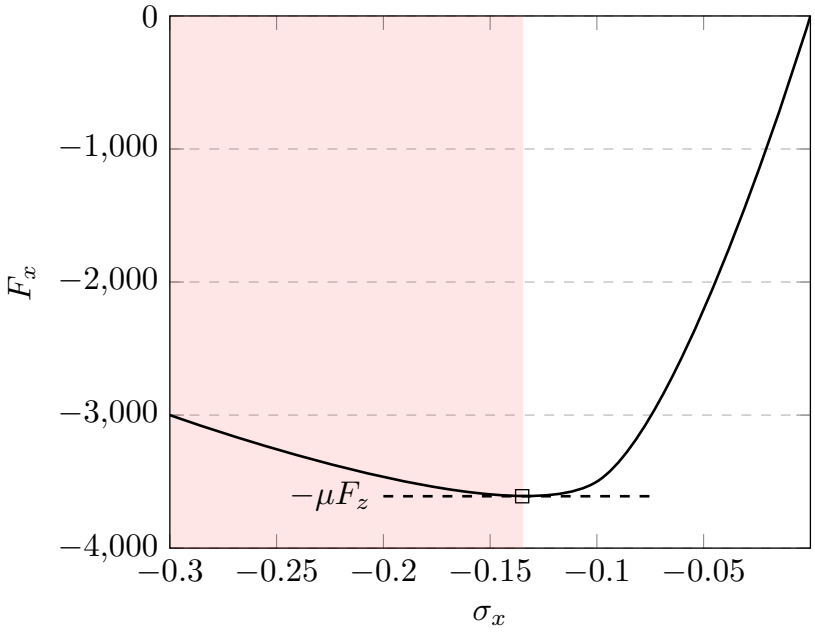

Figure 3.2: Longitudinal force as a function of the slip ratio for $F_y = 0$. Indicates the optimal slip ratio value corresponding to maximum braking force, beyond which the sliding/locking of wheels occurs.

To prevent the wheels from locking/sliding a standard ABS controller was implemented based on the principles introduced in [19, pp. 409]. The basic functionality of an ABS system is to ensure the application of maximum available braking force based on road conditions whilst also ensuring that wheel locking is prevented. The maximum braking force that can be applied at each wheels is calculated based on the friction coefficient and the normal force as follows

$$\begin{aligned} F_{x,i}^{max} &= \mu_i F_{z,i} \\ i &\in \{FL, FR, RL, RR\} \end{aligned} \tag{3.1}$$

Using the tanh model, the longitudinal force can be approximated as a function of the slip ratio σ_x, the longitudinal tire stiffness coefficient C_σ, road surface conditions and the total normal load acting on the wheels. To approximate the reference slip ratio at which this maximum force is achieved the model introduced in (2.17) can be rewritten as

$$\sigma_{x,i}^r = \frac{\mu_i F_{z,i}}{C_\sigma} \operatorname{arctanh}(q) \tag{3.2}$$

where q is a high value close to 1. The input to the ABS block is the error between the reference slip ratio $\sigma_{x,i}^r$ calculated using (3.2) and the actual slip ratio at the wheel as well as the requested braking force given by (3.1). The ABS block ensures that maximum braking torque is applied during the braking sequence while preventing

the wheels of the vehicle to lock/slide. It consists of a bang-bang controller which applies maximum torque when the slip ratio is smaller than the reference and zero torque when the slip ratio is higher than the reference. With a simple low pass filter high frequency changes in braking torque requests are eliminated. The resulting total braking torque is applied to the ego vehicle as illustrated in Figure 3.1. The torque at each time step k at each wheel is given as

$$B_{i,k}^{Trq} = p\mu_{i,k}F_{z,i,k}r_w\left(\frac{\Delta t}{\tau + \Delta t}\right) + B_{i,k-1}^{Trq}\left(\frac{\tau}{\tau + \Delta t}\right) \tag{3.3}$$

where, τ is the time constant of the filter and Δt is the sampling time of the simulation. p is a binary constant with values of either 0 or 1 depending on the sign of $\sigma_{x,i}^{diff} = \sigma_{x,i} - \sigma_{x,i}^{r}$, r_w is the wheel radius. The time constant of the low pass filter is adjusted based on the error of the slip ratio values $\sigma_{x,i}^{diff}$. This ensures that the ABS applies maximum braking torque while also ensuring the slip ratio values do not get saturated. The range of selected values is $\tau \in \{0.08, 2.5\}$ depending on the error in slip ratio.

3.2.2 Lateral Controller

When applying different brake forces on both sides of the vehicle a yaw moment is induced. This leads to a turning motion of the vehicle which could lead to loss of control and the vehicle leaving the lane or even the road. To prevent this behavior a steering controller is implemented to keep the vehicle stable in the lane during the braking maneuver and that counter steers quickly when yaw motion occurs. The Lateral "Stanley" controller, named after the vehicle on which it was implemented during the DARPA Grand Challenge 2005, was proposed in [20] and shows robust performance in lateral control and low cross-track errors. The controller gives a steering input $\delta(t)$ to the vehicle such that the difference between the yaw angle $\Psi(t)$ and a reference yaw angle $\Psi^r(t)$ is minimized as well as the lateral distance to a reference path $e(t) = s_y(t) - s_y^r(t)$. The control law is derived based on kinematic equations of motions which are subsequently augmented to take the system dynamics and non-linearities into account. In the given emergency braking scenario, the vehicle shall be kept within the driving lane with a reference yaw angle of $\Psi^r(t) = 0$ and a lateral reference $s_y(t) = 0$. The control law can, therefore, be simplified and it gives the steering output as

$$\delta(t) = k_p\Psi(t) + \arctan\left(\frac{k_e e(t)}{k_{soft} + v(t)}\right) + k_{dp}\dot{\Psi}(t) \tag{3.4}$$

for $|\delta(t)| \leq \delta_{max}$. For $v(t) > 0$ and $0 < \delta_{max} < \frac{\pi}{2}$ this closed loop system has a globally asymptotic stable equilibrium at $e = 0$ which enables stable lateral control of the plant. The tuning gain k_{soft} is added to make the control more robust at low driving speeds. The value was defined as $k_{soft} = 1\frac{m}{s}$ which showed good results in simulations. Furthermore the paper suggests additions to the control law to compensate for delay in the steering servo motors and reduced tire damping forces in steering actions. These additions will be neglected in the further investigation.

3.3 Decision Making for AEB

A crucial task in an AEB system is to determine the last point at which an emergency brake can be deployed such that a collision is prevented. Often the AEB will be activated when the time to collision (TTC) falls below a certain threshold value [21], [22], [23]. The TTC is defined as presented earlier in (2.23). The threshold time can be approximated by assuming some maximum acceleration based on the given road conditions and ego vehicle velocity. For constant road friction conditions along the ego vehicle's braking path, this threshold can be estimated from the vehicle's kinetic energy [17]. For varying friction profiles along the ego vehicle's braking path, the equation can not be applied anymore as the friction value is now a function of position, i.e. $\mu(s)$. Therefore depending on the threat vehicle's position and the available road friction, the threshold would change.

For this reason, this thesis proposes a novel brake distance estimation algorithm that takes a varying friction profile ahead of the vehicle into account and outputs the last point to brake $x_{brk}(\mu)$ as a function of the friction. This last point to brake is the threat metric which is used instead of the TTC. Based on the current ego and threat vehicle states the Decision Maker will output a braking flag to the longitudinal controller to initiate the braking sequence (Figure 3.3).

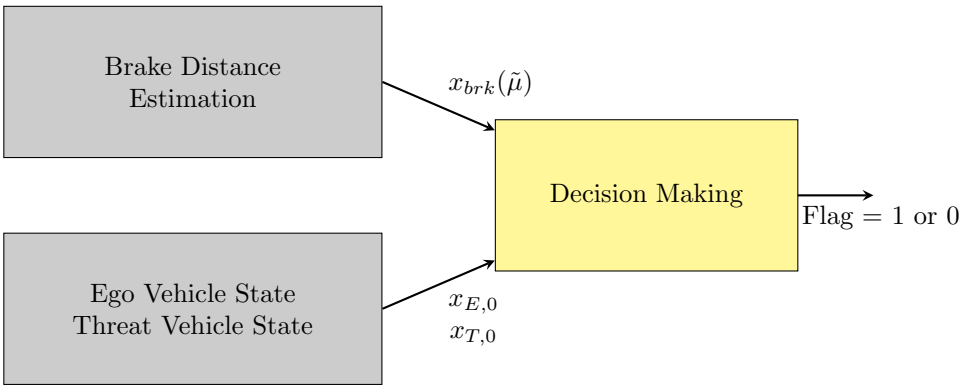

Figure 3.3: Decision Making Structure in proposed AEB system

A general notation shall be defined, $\square_i$ where $\square$ is a placeholder for different physical variables and $i \in \{E, T\}$ refers to either the ego vehicle or the target vehicle. The aim of the algorithm is to determine the last position at which the ego vehicle can trigger an emergency brake, given a predicted friction profile $\tilde{\mu}$, to prevent a collision with a threat vehicle. The ego vehicles initial velocity is given as $v_{E,0}$.

3.3.1 Simulation of Vehicle Motion

To evaluate a given braking point candidate $x_{E,0}$, a simulation of the ego and threat vehicle motion is performed based on the vehicle model (see Section 3.3.3). In each simulation step, the maximum braking force is applied to the ego vehicle. The varying friction profile $\tilde{\mu}$ influences the maximum braking force F_x, which can be applied in each time step as a result of the circle of forces where $F_x \leq \sqrt{(\mu F_z)^2 - F_y^2}$.

Therefore, the braking distance will vary depending on the start point of the braking sequence and the corresponding friction profile ahead of the vehicle. This simulation continues until the point where the velocity of the ego vehicle v_E is smaller or equal to the constant velocity of the threat vehicle v_T.
The threat vehicle is assumed to be stationary or moving with constant velocity. For a velocity $v_T > 0$ the final position of the target is given by $h(x_{T,0}) = x_{T,f}$. In every iteration, it is checked if the ego vehicle reaches the threat vehicle's position and therefore causes a collision or not. In case of a collision, the simulation will output an infeasibility flag as a collision could not be prevented from the given braking point even when applying maximum force. If the ego vehicle reduces its velocity successfully below v_T the simulation outputs the end position $x_{E,f}$ at which the ego vehicle reaches v_T as well as the position of the threat at that time $x_{T,f}$. This simulation of the braking sequence of the ego vehicle is defined as $g(x_{E,0}, \tilde{\mu}) = x_{E,f}$ (see Figure 3.4).

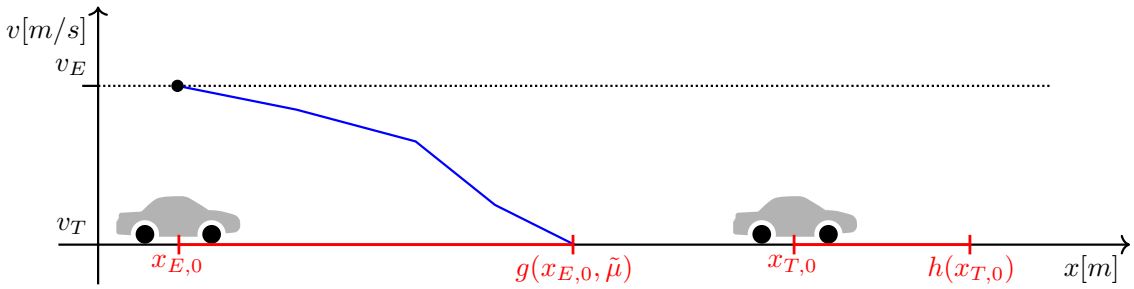

Figure 3.4: Visualization of g and h as functions of the ego and threat vehicle's initial positions $x_{E,0}$ and $x_{T,0}$ as well as the given friction profile ahead $\tilde{\mu}$

3.3.2 Optimization of the last time to brake

To approximate the last braking time instant $x_{E,0}$ of the ego vehicle given a predicted varying friction profile $\tilde{\mu}$ an optimization algorithm based on the bisection method is applied. The optimization problem is formulated as:

$$\text{minimize } f(x_{E,0}, x_{T,0}, \tilde{\mu}) = h(x_{T,0}) - g(x_{E,0}, \tilde{\mu}). \tag{3.5}$$

The feasible set C consists of all points $x_{E,0}, x_{T,0} \in \mathcal{X}$ for which $f(x_{E,0}, x_{T,0}, \tilde{\mu}) \geq 0$ holds i.e., all points for which the ego vehicle reaches v_T without colliding with the stationary vehicle.
A worst case braking distance is determined as the braking distance d for constant friction of $\mu = 0.1$. The best case braking distance is defined as zero. The value of $f(x_{E,0}, x_{T,0}, \tilde{\mu})$ is evaluated in the middle of the chosen best case and worst case data points. Based on the sign of the function evaluation, one of the sub-intervals is disregarded and a new middle point is generated (see Figure 3.5).

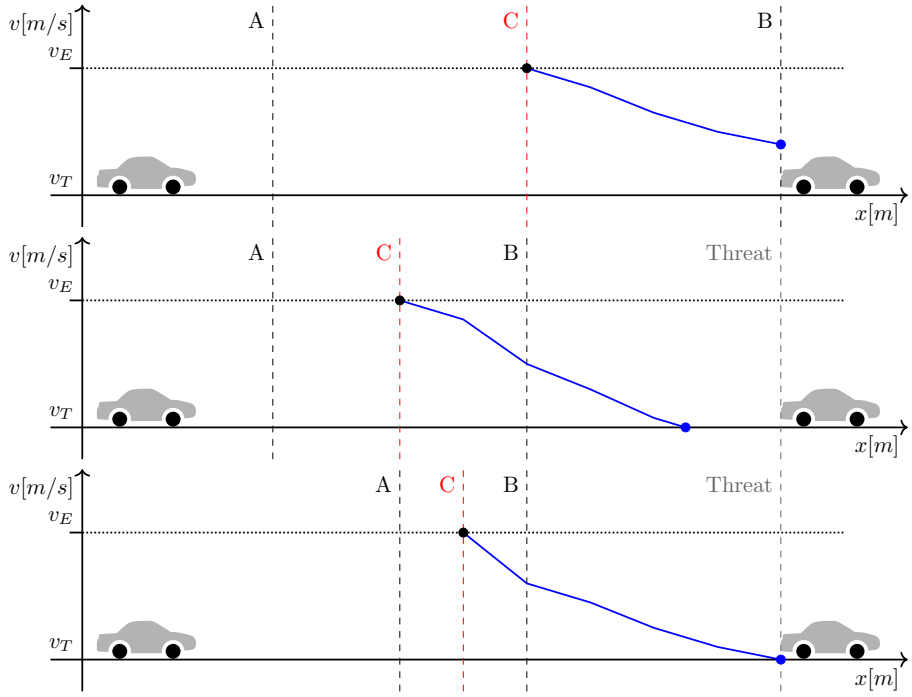

Figure 3.5: Application of bisection method based on brake simulation results

Algorithm 1 Bisection method for brake distance

Define the lower and upper limits as:
A = $x_{T,0} - d$
B = $x_{T,0}$
while $N \leq N_{max}$ **do**
  Calculate middle point between A and B
  C = (A + B)/2
  if $f(C, x_{T,0}, \tilde{\mu}) = 0$ or (B - A) $\leq$ tolerance **then**
    Solution found and Output C
  else
    $N = N + 1$
    if $f(C, x_{T,0}) > 0$ **then**
      B = C
    else
      A = C
    end if
  end if
end while

The algorithm keeps iterating till the starting point for the braking sequence converges to the last point to brake for a finite number of iterations of the bisection method. The last point to brake $x_{brk}(\tilde{\mu})$ is defined as the instance to initiate a braking sequence such that a collision is prevented. The optimization pseudo code is presented in Algorithm 1.

3.3.3 Ego Vehicle Motion Model

A vehicle motion model is used to predict the state of the ego vehicle during the braking sequence. In the course of the optimization framework, the vehicle motion is simulated repeatedly. To reduce computational complexity a simple vehicle model has been developed which enables online computation of the last point to brake. The model is based on a 4-wheel model reduced to longitudinal motion. Several approximations and modifications are introduced to ensure accurate predictions in braking distance while retaining computational speed. The braking motion is described by (3.6) where $F_{x,ij}$ with $i \in \{F, R\}$ and $j \in \{L, R\}$ is the braking force at each wheel and described in the next subsection.

$$a_x = \frac{1}{m}(F_{x,FL} + F_{x,FR} + F_{x,RL} + F_{x,RR}). \tag{3.6}$$

The braking forces $F_{x,ij}$ are determined based on the friction values present at the wheels in each time step (Figure 3.6).

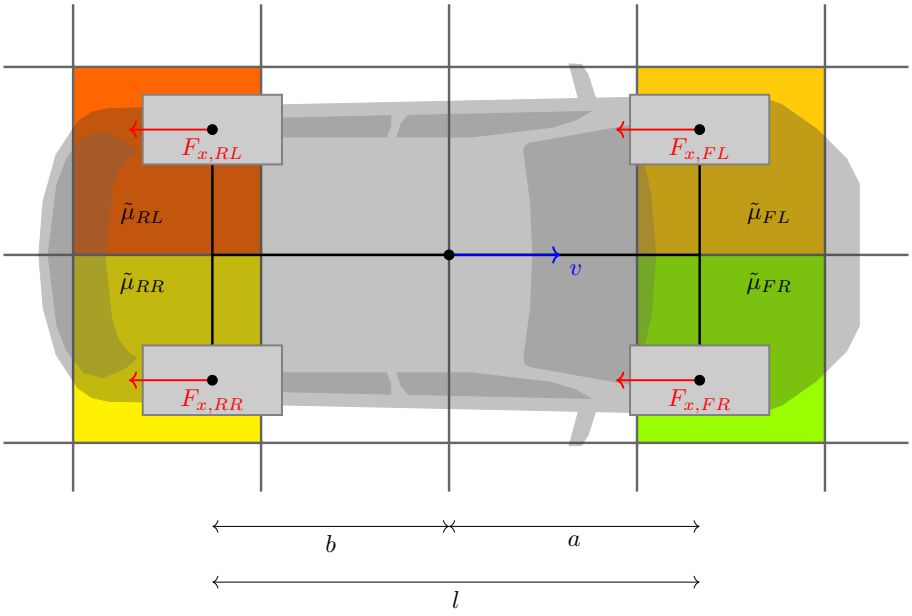

Figure 3.6: Simplified two-track model and $\tilde{\mu}$-cell selection

3.3.4 Maximum Longitudinal Forces

The applied longitudinal braking forces on all tires shall be calculated as the maximum force which can be applied individually to each wheel at each time instance based on friction and normal force as follows:

$$F_{x,ij}^{max} = (\mu_{ij} + f_r)F_{z,ij} \tag{3.7}$$

where f_r is the rolling resistance coefficient, which is used to model the rolling resistance approximately, as a linear function for normal load. Typical values of f_r vary from 0.01 to 0.04. For the simulation setup a value of $f_r = 0.0201$ was chosen for optimal results as in [6, pp. 104].

To accurately capture the forces acting on the vehicle during deceleration, additional modeling/modifications are required to compensate for the simplified model. These include the effects of longitudinal load transfer, brake actuator time delay, existing lateral force due to tire alignment, lateral force compensation.

3.3.4.1 Longitudinal Load transfer

The longitudinal load transfer ($\Delta F_{z,long}$) is modelled as a function of longitudinal acceleration in the vehicle frame as introduced in Section 2.2.2.2. The influence of load transfer on the normal forces can be approximated as:

$$\begin{aligned} \Delta F_{z,long} &= \frac{m a_x h}{l} \\ F_{z,Fi} &= 0.5(\frac{mgb}{l} - \Delta F_{z,long}) \\ F_{z,Ri} &= 0.5(\frac{mga}{l} + \Delta F_{z,long}), \end{aligned} \tag{3.8}$$

with $i \in \{L, R\}$, where m is the vehicle mass, a and b the distance from the CoG to the front and rear axis respectively, l the vehicle length i.e., $a + b$ and g the gravitational acceleration.

3.3.4.2 Actuator Delay

Real braking systems have a build-up phase in which the pressure in the brakes is increased until the requested braking torque is available. To account for this delay in the availability of braking force a delay time t_d is implemented in the calculation of the braking force with a binary coefficient κ. The modified total longitudinal force on the front and rear is:

$$\begin{aligned} F_{x,Fi}^{max} &= \frac{1}{2}(\kappa \mu_{Fi} + f_r) F_{z,Fi} \\ F_{x,Ri}^{max} &= \frac{1}{2}(\kappa \mu_{Ri} + f_r) F_{z,Ri}, \quad i \in \{L, R\} \end{aligned} \tag{3.9}$$

where κ takes a value of 0 or 1 based on the time step k in the simulation.

$$\kappa = \begin{cases} 0 & \text{for } k\Delta t <= t_d \\ 1 & \text{otherwise} \end{cases} \tag{3.10}$$

3.3.4.3 Camber and Toe Angle Compensation

In the simplified model, the simulation of lateral forces is neglected for the sake of decreasing computational complexity, though the real vehicle does experience lateral forces at the wheel even in straight driving scenarios. These forces are induced by camber and toe angles in the vehicle suspension [24, p. 44-45]. These lateral forces limit the total braking forces, which can be applied by the ego vehicle and should therefore also be accounted for by the simplified model. Thus, the calculated

maximum braking force (3.9) is limited using the lateral forces which are measured at the wheels $\hat{F}_{y,Fi}$ and $\hat{F}_{y,Ri}$ of the ego vehicle:

$$\begin{aligned} F_{x,Fi}^{lim} &= \sqrt{F_{x,Fi}^{max2} - \hat{F}_{y,Fi}^{2}} \\ F_{x,Ri}^{lim} &= \sqrt{F_{x,Ri}^{max2} - \hat{F}_{y,Ri}^{2}} \end{aligned} \tag{3.11}$$

3.3.4.4 Lateral Forces Compensation

The occurrence of lateral forces when applying braking input to the ego vehicle has been neglected for the sake of reducing complexity in the model. The simplified model does not keep track of yaw motion or lateral displacement in the course of the braking sequence. In scenarios with differing friction values on the left and right side of the ego-vehicle, lateral forces are induced that limit the total braking force. If this reduction in braking force is not accounted for, the model will become less accurate and prediction performance will decrease.
As steering input is used to counteract yaw torque the actual lateral forces of the ego vehicle are bound. Therefore, a simple compensation of the induced forces can be added without keeping track of the actual yaw momentum to account for this issue. The car's yaw moment of inertia considering no steering is given by

$$\begin{aligned} J\ddot{\Psi} =& a(F_{y,FL} + F_{y,FL}) - b(F_{y,RL} + F_{y,RR}) + \\ & \frac{w}{2} \underbrace{(F_{x,FR} - F_{x,FL} + F_{x,RR} - F_{x,RL})}_{F_{x,diff}}. \end{aligned} \tag{3.12}$$

In a straight driving scenario a yaw moment is therefore mainly induced by $F_{x,diff}$, the difference in longitudinal forces on the left and right side of the vehicle. The difference in friction values on either side of the vehicle can therefore be used as an approximation of the lateral force which is induced. A compensation value K_{Lat} is proposed which reduces the amount of longitudinal force F_x which is applied based on the difference in μ. It is calculated by the equation

$$K_{Lat} = p(\underbrace{\mu_{FR} - \mu_{FL} + \mu_{RR} - \mu_{RL}}_{\mu_{diff}})^2 \tag{3.13}$$

with a tuning gain p and limited to $0 \leq K_{Lat} \leq 0.1$. For the given vehicle and controller a gain of $p = 0.2$ showed good results in simulations. With this compensation factor the final longitudinal forces for front and rear in the open loop simulations are given as:

$$\begin{aligned} F_{x,Fi} &= (1 - K_{Lat}) F_{x,Fi}^{lim} \\ F_{x,Ri} &= (1 - K_{Lat}) F_{x,Ri}^{lim}. \end{aligned} \tag{3.14}$$

With the introduced algorithm and vehicle model, an autonomous braking maneuver can be deployed on various road surface conditions based on predicted friction information. In certain situations, though it might not be possible to prevent collisions by braking due to the proximity to the threat vehicle or very low friction. In these cases, an autonomous emergency steering can be used to avoid a collision.

4

Autonomous Emergency Steering

In this chapter the utilization of road friction information in emergency lane change scenarios is detailed. The problem is formulated to determine the last point to initiate a lane change maneuver by utilizing the maximum available lateral forces based on the road friction information. Two approaches are described here which use road friction information to enable a lane change maneuver which is: model predictive control and curve-based path planning.

4.1 Emergency lane change system architecture

The objective in a lane change scenario is for the ego vehicle to move to the adjacent lane under certain constraints. To safely execute a lane change maneuver, the vehicle must be able to compute a safe trajectory that respects the limitations set by the road conditions and the vehicle system limitations in terms of maximum lateral and longitudinal acceleration and the total forces acting on the tires. Figure 4.1 shows the block diagram of the system architecture for an AES system.

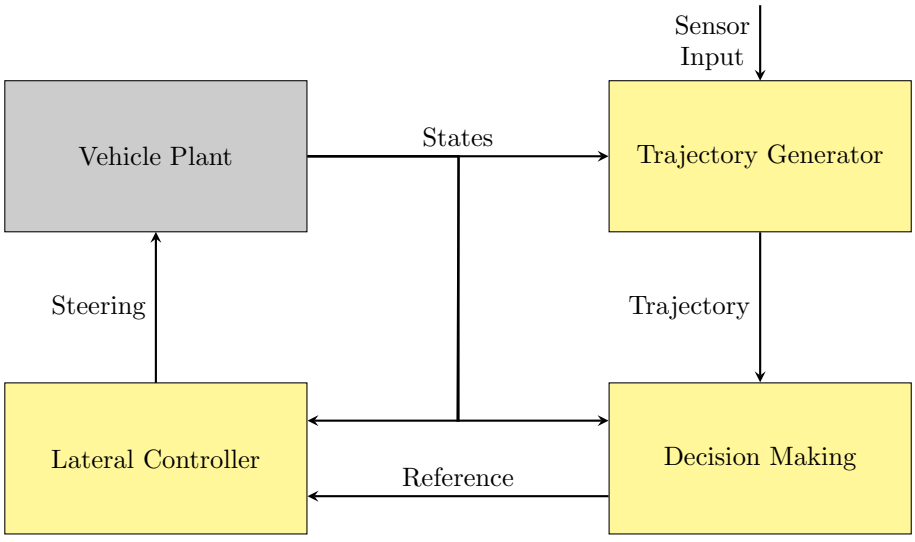

Figure 4.1: System Architecture AES

The Autonomous Emergency Steering system mainly consists of:

- **Trajectory Generator** - Computes the lane change trajectory corresponding to the last point $x_{E,0}$ to start a lane change.

- **Decision Making** -The decision making block evaluates he current ego and threat vehicle position and hands over the generated trajectory to the controller when $x_{E,0}$ is reached.
- **Lateral controller** - A path tracking controller using steering control guides the vehicle along the computed path.

The two investigated approaches implement these function blocks to different extents. While the curve-based path planning approach has separate algorithms which realize trajectory planning, decision making and lateral control, the model predictive control-based approach combines all these functions in one.

4.2 Model Predictive Control for Emergency Steering

In this chapter the control strategy of model predictive control (MPC) is introduced and its application to the problem of autonomous emergency steering in dynamic friction environments.

4.2.1 Introduction to MPC

The fundamental principle of Model Predictive Control (MPC) is to use dynamic models to predict the behaviour of a system and determine an optimal control input for the current time [25, p. 1]. The optimal control input is found by minimizing an objective function. MPC proposes an interesting solution to the control problem in many applications as it is possible to incorporate constraints on the system dynamics and the control inputs as part of minimizing the objective function and delivers an optimal solution. While the computationally expensive calculation of control inputs made MPC for many years mainly suitable for slow processes, the progress in computer hardware made the use also in automotive applications possible [26, pp. 5].

A vehicle model suitable for the problem description is necessary to accurately forecast the system evolution over a finite amount of time steps. Depending on the problem at hand different vehicle models can be used, a variety of models have been described in Section 2.2. As presented, linear and nonlinear models exist and can predict the vehicle motion to varying degree of accuracy depending on the chosen scenario. The advantage of using linear models is that they are relatively easy to solve and in combination with quadratic objective functions result in convex problems [26, p. 249]. Convex problems are preferred as they have one distinct optimum and there exist many commercial solutions to solve them. However the linear MPC can not be applied to scenarios where the nonlinear nature of the vehicle dynamics leads the system away from steady state set points which can be chosen for linearization. In these cases a nonlinear model has to be applied.

Linear MPC models are known to be used in lane change and emergency steering application with many successful implentations [27], [28]. The common premise is that for the limited degrees of freedom in a lane change scenario a linear model like

the one described in Section 2.2.2.1 is sufficient as the longitudinal velocity can be assumed constant and steering angles close to zero. A disadvantage with these linear models is the depiction of tire forces as linear functions of the slip ratio and the slip angle. For scenarios where forces at the limit of tire saturation shall be applied these models can not accurately determine the tire forces which will decrease the prediction accuracy. Furthermore in the given case a varying friction profile of the form presented in Figure 2.1 is assumed which implies that at each time instance each wheel can experience a different force and has different limits. To account for these varying friction conditions and to have an accurate representation of the tire forces a nonlinear MPC is used for the given task.

Typically a nonlinear MPC regulator determines the next control action by minimizing a cost function of the general form

$$\begin{aligned} \min_{x,u} J(x,u) = & \sum_{k=0}^{N-1} x_k^T Q x_k + u_k^T R u_k + x_N^T Q_N x_N, \\ s.t. \quad & x_{k+1} = f(x_k, u_k), \text{ for } k = 1, ..., N-1 \\ & g(x_k, u_k) \leq 0, \text{ for } k = 1, ..., N-1 \end{aligned} \tag{4.1}$$

where x is the state vector, u is the control input and N is the horizon length i.e. the amount of time steps which the MPC predicts into the future. Q, R and Q_N are weighting factors which define the influence of each state on the final cost. A terminal constraint of $x_N = 0$ ensures stability of the achieved solution [26, p. 279], by increasing the cost factor Q_N it can be ensured that $x_N \to 0$. Constraints on the values of x and u are defined by $f(x_k, u_k)$ and $g(x_k, u_k)$.

4.2.2 Related Work

Several approaches are known to let the road friction influence the behaviour of the MPC framework. The work in [29] proposes a system which is based on an online estimation of the friction value under the vehicle and the prediction of the vehicle behaviour using an accurate tire model. The complex semi-empirical Pacejka model [13] is used to accurately estimate the tire forces and keep the vehicle stable close to a reference trajectory. The work in [30] uses the prediction of lateral tire forces with a simplified model to constraint the applied force in each time step. This is done to stabilize the vehicle also in the presence of low friction road surfaces.The system proposed in [31] finally uses an online estimation of tire parameters in the Pacejka model to achieve a friction-adaptive nonlinear MPC regulator. The controller is designed to be robust against low friction road surfaces and is able to accurately adjust the tire force estimation online.

Common assumptions that are made in the mentioned works are that *(i)* the future friction values are not known, *(ii)* the current friction estimation stays constant over the prediction horizon, *(iii)* the friction is constant on all four wheels. This thesis shall investigate the performance of the MPC framework for the case when future friction values are provided in the form presented in Section 2.1.3. The contribution

is therefore the investigation of MPC emergency steering performance with varying friction values on all four wheels of the vehicle.

4.2.3 Vehicle Model

In the MPC framework the vehicle dynamics are enforced as an equality constraint on the state vector by $x_{k+1} = f(x_k, u_k)$. The formerly introduced models have to be slightly adjusted for the purpose of the MPC. A vehicle model based on the 3 DOF 4-wheel model introduced in Section 2.2.3 shall be used. As in the case of the lane change maneuver no braking or acceleration force is applied, the longitudinal forces in the model can be neglected. The resulting equations of motion are

$$\begin{aligned} ma_x &= -(F_{y,FL} + F_{y,FR})sin(\delta) \\ ma_y &= F_{y,RL} + F_{y,RR} + (F_{y,FL} + F_{y,FR})cos(\delta) \\ J\ddot{\Psi} &= \left\{ \begin{array}{r} acos(\delta)(F_{y,FL} + F_{y,FL}) \\ -b(F_{y,RL} + F_{y,RR}) \\ +\frac{w}{2}sin(\delta)(F_{y,FL} - F_{y,FR}) \end{array} \right\}. \end{aligned} \tag{4.2}$$

The state vector is chosen as

$$x = \begin{bmatrix} s_{x,wf} \\ \dot{s}_x \\ s_{y,wf} \\ \dot{s}_y \\ \Psi \\ \dot{\Psi} \end{bmatrix}, \tag{4.3}$$

where $s_{x,wf}$ and $s_{y,wf}$ are the s_x and s_y position of the vehicle COG in world frame coordinates. $s_{x,wf}$ and $s_{y,wf}$ are obtained by multiplying s_x and s_y, the vehicle coordinates in vehicle frame coordinates, with the rotation matrix R

$$R = \begin{bmatrix} cos(\Psi) & -sin(\Psi) \\ sin(\Psi) & cos(\Psi) \end{bmatrix}. \tag{4.4}$$

The input u to this model is the steering angle δ. This setup allows the enforcement of constraints on the global position of the vehicle based on the the position of the threat vehicle as described in the following Section 4.2.4.

The tire model is based on the tanh approximation presented in Section 2.2.4. This tire model gives a good approximation of the actual tire dynamics as long as the tire is not saturated. As the tire forces can be limited using constraints as part of the MPC (see Section 4.2.6), this approximation gives a realistic representation of the tire state while keeping computational complexity low. As shown in (4.5), the friction at each tire influences the lateral force at each tire independently.

$$F_{y,i} = \mu_i F_{z,i} \tanh\left(\frac{C\alpha_i}{\mu_i F_{z,i}}\right), \quad i \in \{FL, FR, RL, RR\} \tag{4.5}$$

The described continuous system in (4.2) is discretized for the MPC using Euler backward method with sampling time Δt.

$$\begin{aligned} \dot{x} &\approx \frac{x_{k+1} - x_k}{\Delta t} \\ \Leftrightarrow x_{k+1} &= x_k + \Delta t \dot{x} = f(x_k, \delta_k) \end{aligned} \tag{4.6}$$

4.2.4 Obstacle Avoidance

Emergency steering and obstacle avoidance using MPC regulators are well researched topics [27], [28], [29], [32]. A common way to implement obstacle avoidance is to frame the obstacle as a constraint on the lateral position of the vehicle. For this the vehicle coordinates s_x and s_y are projected into the world frame of the road giving $s_{x,wf}$ and $s_{y,wf}$. With these coordinates the distance to the center of the road can be calculated for every time step of the MPC prediction. The distance is calculated as

$$e_y = s_{y,wf} - s_{y,c}, \tag{4.7}$$

where $s_{y,c}$ is the lateral center of the road. Given the position of the obstacle this can be used to set a constraint on the distance from the center of the road and therefore force the MPC to avoid the obstacle (see Figure 4.2).

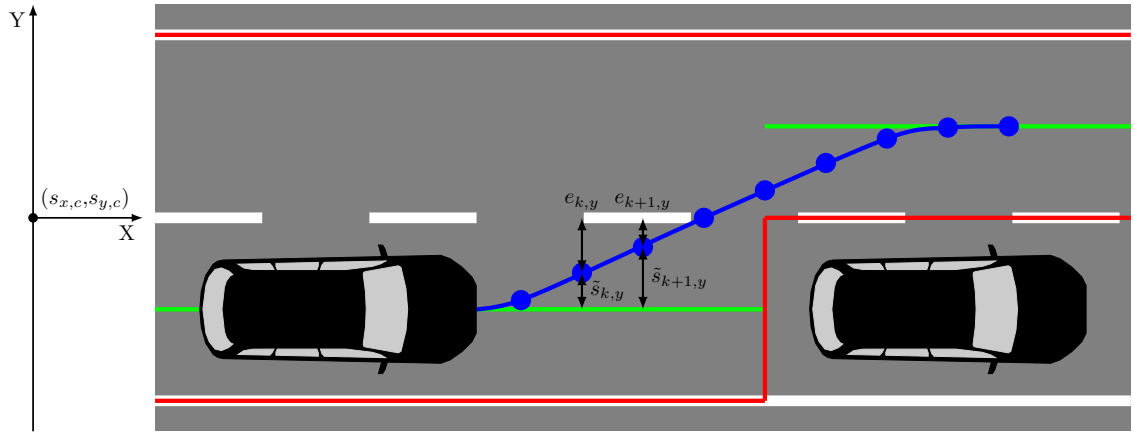

Figure 4.2: Constraints on lateral ego vehicle position (red), predicted lateral position (blue) and lateral reference (green)

Based on the introduced concepts the obstacle avoidance can be implemented by setting a linear constraint on e_y

$$e_{k,y}^{min} \leq e_y \leq e_y^{max}. \tag{4.8}$$

The value of e_y^{max} is constant and defined by the upper road boundary. The value of $e_{k,y}^{min}$ is set to the lower road boundary until the obstacle is within the range of the prediction horizon. For every time step where the predicted position of the ego vehicle's front bumper is greater or equal than the longitudinal position of the

threat vehicle's rear bumper, the value of $e_{k,y}^{min}$ is changed. A safety value $s_{x,safety}$ can be added to change the lower boundary earlier and account for inaccuracies in the MPC calculation. The value of $e_{k,y}^{min}$ is changed to

$$e_{k,y}^{min} = L_r + \frac{w_E}{2} + \frac{w_T}{2} + s_{y,safety} \tag{4.9}$$

where L_r is the lateral coordinate of the right lane center, w_E is the width of the ego vehicle chassis, w_T is the threat vehicle's chassis width and $s_{y,safety}$ is an added safety distance.
As with the given setup the MPC will try to solve for a trajectory close to the constraint borders, small modeling inaccuracies or unknown disturbances can lead to infeasible solutions. A way to regain feasibility is to turn the hard constraint in (4.8) into a soft constraint [31] of the form

$$e_y^{min} - \varepsilon \leq e_y \leq e_y^{max}. \tag{4.10}$$

The newly introduced variable $\varepsilon \geq 0$ changes the lower limit on e_y and therefore allows the MPC to violate e_y^{min} in order to achieve a feasible solution. To prevent high violations of e_y^{min}, ε is included in the cost function with a high penalty (introduced in Section 4.2.7). This way it can be ensured that it is only bigger than zero when it is necessary to find a feasible solution. In matrix form (4.10) yields

$$\begin{bmatrix} I \\ -I \end{bmatrix} \mathbf{e}_y \leq \begin{bmatrix} \mathbf{e}_y^{max} \\ -\mathbf{e}_y^{min} + \boldsymbol{\varepsilon} \end{bmatrix} \tag{4.11}$$

with $\mathbf{e}_y$, $\mathbf{e}_y^{max}$, $\mathbf{e}_y^{min}$ and $\boldsymbol{\varepsilon}$ defined as

$$\mathbf{e}_y = \begin{bmatrix} e_{0,y} \\ \vdots \\ e_{N-1,y} \end{bmatrix}, \quad \mathbf{e}_y^{max} = \begin{bmatrix} e_y^{max} \\ \vdots \\ e_y^{max} \end{bmatrix}, \quad \mathbf{e}_y^{min} = \begin{bmatrix} e_{0,y}^{min} \\ \vdots \\ e_{N-1,y}^{min} \end{bmatrix}, \quad \boldsymbol{\varepsilon} = \begin{bmatrix} \varepsilon_0 \\ \vdots \\ \varepsilon_{N-1} \end{bmatrix}. \tag{4.12}$$

In a compact form this shall be referred to as

$$H_{obs}\boldsymbol{x} - h_{obs} \leq \boldsymbol{\varepsilon}. \tag{4.13}$$

Given this obstacle avoidance implementation the MPC is not dependent on a separate decision making algorithm. As soon as an obstacle is detected it will solve for a feasible trajectory and follow it, therefore initiating the lane change without an external input. The MPC can be used to follow a reference while making sure not to violate the given constraints on e_y by changing the cost function such that it minimizes the difference between the state and the reference

$$\tilde{s}_y = s_{y,wf} - s_y^r. \tag{4.14}$$

If no pre-generated trajectory is available the MPC can be utilized for the generation of an optimal trajectory [27], [32]. As the MPC is calculating an optimal control sequence given a certain cost function and constraints it can generate a feasible trajectory which avoids the obstacle while staying close to some constant reference. To achieve a smooth lane change the reference is changed from the middle of the right lane to the middle of the left lane as soon as the obstacle is reached (see Figure 4.2).

4.2.5 System Constraints

Based on the cost function and vehicle model described in the previous sections, the MPC will generate a lane change trajectory without taking acceleration and actuator constraints into account. To enforce the physical system limits in the MPC calculation, these are framed as constraints on state x and input δ. The upper and lower limits of the steering angle δ^{min} and δ^{max} are enforced by a linear constraint on the steering input

$$\delta^{min} \leq \delta \leq \delta^{max}. \tag{4.15}$$

In matrix form this yields

$$\begin{bmatrix} I \\ -I \end{bmatrix} \boldsymbol{\delta} \leq \begin{bmatrix} \boldsymbol{\delta}^{max} \\ -\boldsymbol{\delta}^{min} \end{bmatrix} \tag{4.16}$$

with $\boldsymbol{\delta}$, $\boldsymbol{\delta}^{max}$ and $\boldsymbol{\delta}^{min}$ defined as

$$\boldsymbol{\delta} = \begin{bmatrix} \delta_0 \\ \vdots \\ \delta_{N-1} \end{bmatrix}, \quad \boldsymbol{\delta}^{max} = \begin{bmatrix} \delta^{max} \\ \vdots \\ \delta^{max} \end{bmatrix}, \quad \boldsymbol{\delta}^{min} = \begin{bmatrix} \delta_0^{min} \\ \vdots \\ \delta_{N-1}^{min} \end{bmatrix} \tag{4.17}$$

While the values of $\boldsymbol{\delta}^{max}$ are constant based on the system limit for steering angle the values of $\boldsymbol{\delta}^{min}$ can change over time. By enforcing varying limits on the minimum steering angle that can be applied, the trajectory generation of the MPC can be influenced. An issue which shall be addressed with this specifically is the prevention of unnecessary oscillatory behaviour in the initiation of a lane change maneuver. Figure 4.3a shows the beginning of a lane change maneuver trajectory with a constant value of δ^{min} at the system limit. As it can be seen the MPC delivers a solution with several changes in steering direction before the lane change is actually initiated. This behaviour is undesirable as it imposes forces on the tires and causes an unnecessarily early intervention of the autonomous system.

Different methods can be used to tackle this issue. A straight forward solution is to increase the cost for changes of the steering direction. This can successfully lead to a smoother trajectory without the shown behaviour. A downside of this solution is that by increasing the cost on steering changes, the cost on deviations from the reference relatively decreases which leads to an earlier triggering of the lane change. To achieve both, a smooth lane change as well as close reference tracking, the introduced change of the minimum steering limit can be used. By setting δ_k^{min} to a negative value close to zero in the initiation of a lane change sequence it can be prevented that the system applies large negative steering. When the threat vehicle is close, the value of δ_k^{min} is changed back to the actual system limit to allow negative steering onto the left lane. With this change a smooth lane change is achieved as Figure 4.3b illustrates.

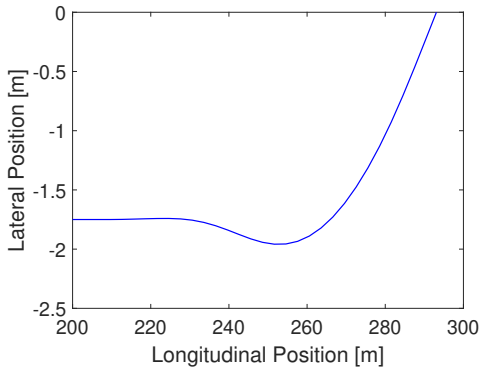

(a) Initiation of lane change sequence with constant δ^{min} at system limit

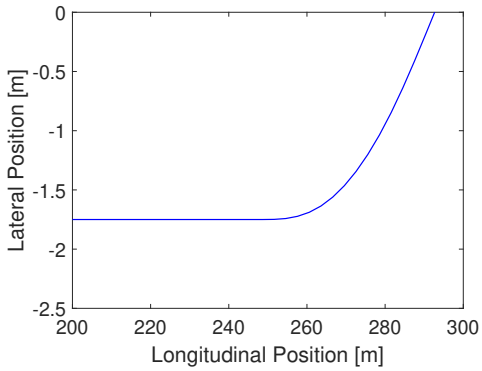

(b) Initiation of lane change sequence with dynamic δ^{min}

Figure 4.3: Illustration of the influence of a dynamic lower steering limit on the trajectory generation in the lane change scenario

The steering rate $\dot{\delta}$ is obtained by solving the finite difference approximation for the change of δ within one time step Δt. Therefore $\dot{\delta}$ is given by

$$\dot{\delta}_k = \frac{\delta_k - \delta_{k-1}}{\Delta t}. \tag{4.18}$$

The constraint becomes

$$\dot{\delta}^{min} \leq \frac{\delta_k - \delta_{k-1}}{\Delta t} \leq \dot{\delta}^{max}. \tag{4.19}$$

For $k = 0$ the constraint in matrix form is

$$\begin{bmatrix} 1 & 0 & \dots & 0 \\ -1 & 0 & \dots & 0 \end{bmatrix} \boldsymbol{\delta} \leq \begin{bmatrix} \dot{\delta}^{max} + \delta_{-1} \\ -\dot{\delta}^{min} - \delta_{-1} \end{bmatrix} \tag{4.20}$$

where δ_{-1} is the steering input applied in the previous time step. For $k > 1$ the constraint in matrix form is

$$\begin{bmatrix} D \\ -D \end{bmatrix} \boldsymbol{\delta} \leq \begin{bmatrix} D_{max} \\ -D_{min} \end{bmatrix} \tag{4.21}$$

with

$$D = \begin{bmatrix} -1 & 1 & 0 & \dots & 0 \\ 0 & -1 & 1 & \dots & 0 \\ \vdots & & \ddots & \ddots & \\ 0 & \dots & 0 & -1 & 1 \end{bmatrix}, \quad D_{max} = \begin{bmatrix} \dot{\delta}^{max} \\ \vdots \\ \dot{\delta}^{max} \end{bmatrix}, \quad D_{min} = \begin{bmatrix} \dot{\delta}^{min} \\ \vdots \\ \dot{\delta}^{min} \end{bmatrix} \tag{4.22}$$

Equations (4.16),(4.20) and (4.21) are combined to the linear inequality constraint

$$H_{sys}\boldsymbol{\delta} \leq h_{sys} \tag{4.23}$$

Another limitation of the system is the maximum lateral force which can be applied in the course of the lane change maneuver [33]. To constraint the amount of force

applied, a limit is put on the maximum and minimum lateral acceleration of the system

$$a_y^{min} \leq a_y \leq a_y^{max}. \tag{4.24}$$

The lateral acceleration is calculated based on (4.2). As it is not part of the state vector the limitation is implemented as a nonlinear constraint with

$$g_1(x_k, \delta_k) = \begin{bmatrix} a_{ky} - a_y^{max} \\ -a_{k,y} + a_y^{min} \end{bmatrix} \leq 0. \tag{4.25}$$

4.2.6 Friction-based Constraints

In Section 4.2.3 it was shown that a simple tanh model is used for the estimation of tire forces in the proposed MPC. As the simple model only gives a good estimation of the tire dynamics up to the tire saturation, a limit on the forces is necessary to retain accurate predictions of the vehicle behaviour [30].

$$F_{y,i}^{min} \leq F_{y,i} \leq F_{y,i}^{max}, \quad i \in \{FL, FR, RL, RR\} \tag{4.26}$$

The constraints on the lateral forces at each wheel are defined by the normal forces and the friction value. To account for inaccuracies due to the simplified model the force maximum is multiplied with an additional parameter $w = 0.95$. The limits in each time step k as a function of the current friction $\mu_{k,i}$ become

$$\begin{aligned} F_{k,y,i}^{min} &= -w\mu_{k,i}F_{z,i} \\ F_{k,y,i}^{max} &= w\mu_{k,i}F_{z,i}. \end{aligned} \tag{4.27}$$

The friction value $\mu_{k,i}$ is picked in each time step for each wheel depending on the predicted wheel position in the μ-grid. The resulting nonlinear inequality constraint for the lateral forces at each tire is

$$g_2(x_k, \delta_k) = \begin{bmatrix} F_{k,y,i} - F_{k,y,i}^{max} \\ -F_{k,y,i} + F_{k,y,i}^{min} \end{bmatrix} \leq 0. \tag{4.28}$$

4.2.7 Cost Function

A general cost function for a nonlinear MPC was introduced in (4.1). For the specific task of generating and following a lane change trajectory several changes have to be made to the cost function based on the previously introduced principles. Firstly the state vector x is replace in the cost function with the variable $\tilde{x} = x - x^r$ to enable reference tracking. The state reference x^r is zero for all states besides s_y which has the reference s_y^r. Also an additional cost value is defined for change of steering input with tuning value R_d. A high value in R_d shall prevent rapid changes in the steering direction and leads to a smoother trajectory generation. The steering rate in the cost function $\dot{\delta}$ is defined as presented in (4.19). The slack variable ε for the soft constraint on e_y is added with tuning gain E which takes a relatively high value to prevent unnecessary constraint violations.

The system constraints from Equations (4.6), (4.13), (4.23), (4.25) and (4.28) are combined as constraints on the solution to the cost function $J(\tilde{x}, \delta, \varepsilon)$.

$$\begin{aligned} \min_{\tilde{x},\delta,\varepsilon} J(\tilde{x}, \delta, \varepsilon) = & \sum_{k=0}^{N-1} \tilde{x}_k^T Q \tilde{x}_k + \delta_k^T R \delta_k + \dot{\delta}_k^T R_d \dot{\delta}_k + \varepsilon_k^T E \varepsilon_k + x_N^T Q_N x_N, \\ s.t. \quad & H_{obs}\boldsymbol{x} - h_{obs} \leq \boldsymbol{\varepsilon} \\ & \boldsymbol{\varepsilon} \geq 0 \\ & H_{sys}\boldsymbol{\delta} \leq h_{sys} \\ & x_{k+1} = f(x_k, \delta_k), \text{ for } k = 1, ..., N-1 \\ & g_1(x_k, \delta_k) \leq 0, \text{ for } k = 1, ..., N-1 \\ & g_2(x_k, \delta_k) \leq 0, \text{ for } k = 1, ..., N-1 \end{aligned} \tag{4.29}$$

4.3 Curve-based Path Planning for Emergency Steering

To ensure autonomous vehicles are operable in dynamic traffic, path planning and real time trajectory generation play a vital role in the development of autonomous driving. Path planning mainly deals with searching for feasible paths in an environment for the autonomous vehicle to follow. This involves taking into account the kinematic constraints of the vehicle, the geometric constraints induced by the vehicle design and the surroundings that affect the feasibility of the paths. A lot of research has been carried out in the last decade that addresses the path planning problem for autonomous vehicles [34], [35], [36], one part of which is the autonomous lane change maneuver.

Lane change is an important maneuver which is used in many scenarios such as overtaking or merging/exiting a highway. Emergency lane change systems are also developed to meet collision avoidance requirements in ADAS development. For example, in highway driving scenarios an emergency lane change maneuver may be required to avoid a collision when it cannot be avoided by braking [33].

4.3.1 Friction incorporation in path

In a lane change scenario, a common assumption is that there is no braking or longitudinal acceleration involved, therefore the longitudinal forces of the vehicle are ignored. The maximum lateral acceleration assuming a point mass model of the vehicle is then approximated as:

$$a_y^{max} = \mu g \tag{4.30}$$

where, μ is the road friction coefficient and g is the gravity constant. Furthermore an additional restriction based on actual system capabilities is used to limit the maximum permissible lateral acceleration [33]. This maximum lateral acceleration constraint can be used to generate simple lane change maneuvers incorporating the

friction by using for example Quintic polynomial curves [14].

An alternative approach is to include constraints on the maximum curvature of the path [37], [38]. Consider a point mass vehicle model moving in a circular path under constant longitudinal motion Figure 4.4, the total centripetal forces acting on the vehicle is defined by:

$$F_y = \frac{mV^2}{R} \tag{4.31}$$

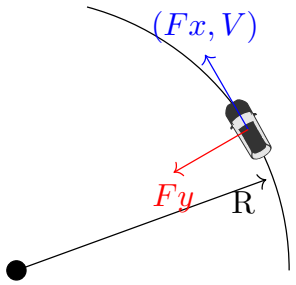

Figure 4.4: Force acting on vehicle moving in a curved path

Where, R is the radius of curvature of the path, m is the mass of the vehicle and V is the directional velocity vector of the vehicle. Further, from total force circle described in Section 2.2.4 it is shown that the total lateral force F_y that can act on the tires is bound by the total normal load and road surface coefficients.

$$\begin{aligned} F_y &\leq \sqrt{F_z^2 - F_x^2} \\ F_y &\leq m\sqrt{\mu^2 g^2 - a_x^2} \end{aligned} \tag{4.32}$$

Combining this with the centripetal force equation we get

$$\begin{aligned} \frac{mV^2}{R} &\leq m\sqrt{\mu^2 g^2 - a_x^2} \\ \frac{1}{R} = k &\leq \frac{\sqrt{\mu^2 g^2 - a_x^2}}{V^2} \\ \frac{1}{R} = k &\leq \frac{\sqrt{\mu^2 g^2}}{V^2} \end{aligned} \tag{4.33}$$

Using the above relation, the maximum curvature of the path is defined and the resulting lane change path is generated using curve based approaches such as clothoids, and Bezier curves [39] [40].

For the scenario in which we have varying friction profiles laterally as shown in Figure 4.5, the total maximum curvature of the resulting path on each lane is different.

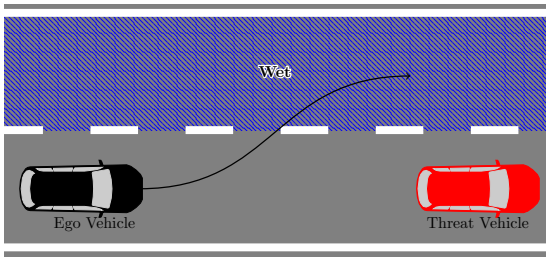

Figure 4.5: Lane change - Laterally varying friction profile

Using the introduced relation for maximum curvature, we define the limits on curvature for each lanes. These are defined as K_R^{max} and K_L^{max} for the right and left lane respectively. Additionally, in order to ensure that the lateral acceleration of the car during lane change does not exceed the bounds set by system limits [33] the maximum acceleration is limited:

$$a_y^{min} \leq a_y \leq a_y^{max} \tag{4.34}$$

The corresponding maximum permissible curvature of the path is calculated based on:

$$\begin{aligned} K_{sys}^{max} &= \frac{a_y^{max}}{V_x^2} \\ |K_i^{max}| &\leq K_{sys}^{max}, i \in (L, R) \end{aligned} \tag{4.35}$$

4.3.2 Related work

There has been a lot of research carried out in generating lane change trajectories with limitations on the maximum permissible lateral acceleration and resulting curvature based on friction. The work carried out in [37] suggests the use of piecewise quadratic Bezier curves to generate a continuous curvature path based on calculated safety distances for the lane change. The authors then evaluate the maximum curvature of the generated path to be within the comfort driving limits of the vehicle in terms of lateral acceleration. Quintic polynomials are another type of curves widely used in lane change trajectory generation due to its simplicity to implement and to incorporate constraints on lateral acceleration [41], [42], [43]. The resulting path from quintic polynomials are continuous in curvature, smooth, and satisfy the lateral acceleration limits.

Alternatively, the work in [39], generates lane change trajectories based on clothoids. The resulting curvature of the generated clothoid is limited based on the available road friction coefficient. Further, the work in [38] proposes the generation of lane change trajectories using clothoids at the limit of friction. This is performed by generating a speed profile of the trajectory which is depending on the curvature of the path and the road friction coefficient. The common assumptions made in the mentioned works are that the friction remains constant throughout the path. This ensures that the maximum limit on lateral acceleration and curvature is constant throughout the generated path.

This thesis shall investigate the performance of a path planning framework when future friction information is made available in the form presented in Section 2.1.3. The main contribution is, therefore, is to study the effect of dynamic road friction profile on lane change trajectories for autonomous emergency steering applications. While any of the continuous curvature path generation techniques discussed can be applied to generate lane change trajectories, Bi-Elementary paths based on clothoids are used in this thesis, mainly due to its simplicity and ability to have direct control over the curvature of the path.

4.3.3 Trajectory Generation

As stated earlier, the main subject of this chapter is trajectory generation or path planning incorporating dynamic friction information. Therefore, the main work contributions belong to the trajectory generation block illustrated in Figure 4.6. The components of the trajectory generation algorithm are shown in Figure 4.6. Information from the sensor about the road conditions, detected threats, and current vehicle state is made available to the trajectory generation block.

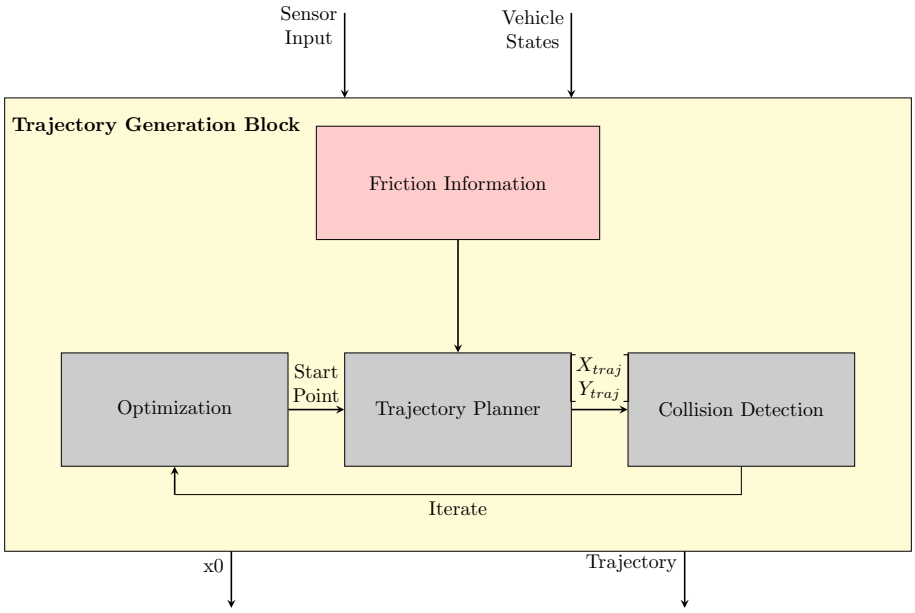

Figure 4.6: Trajectory Generation Block

The trajectory generation consists of 3 core functions:

- **Optimization** - Optimization based on Bisection method similar to AEB described in Section 3.3.2 to determine last point $x_{E,0}$ to start lane change scenario to avoid a collision. More details in Section 4.3.3.1
- **Trajectory Planner** - A clothoid based path planner is used to generate lane change paths and a velocity profile is assigned to the generated path to obtain a trajectory. Given an initial starting position of ego vehicle specified by $x_{E,0}$ the trajectory planner generates a lane change trajectory. More details in Section 4.3.3.2

- **Collision Detection** - Each generated trajectory is checked for possible collision occurrence with detected threat. More Details in Section 4.3.3.6

4.3.3.1 Optimization to determine start point of lane change

To determine the last point $x_{E,0}$ to initiate a lane change maneuver of the ego vehicle considering the varying friction profile $\tilde{\mu}$ an optimization algorithm based on bisection method similar to the AEB explained in Section 3.3.2 is utilized. The details regarding bisection method will not be explained in this section to avoid repetitions and can be referred from the earlier section. The upper and lower limit of the candidate start point of lane change is computed by determining the last point to steer to avoid collision under worst case low friction and high friction conditions using

$$x_{steer} = \sqrt{\frac{2w}{\mu g}}\Delta v. \tag{4.36}$$

Where w is the distance between centers of the two lane, Δv is the relative velocity of the ego with respect to target. The objective function to minimize is the distance between the start point to lane change $x_{E,0}$ and the target position $x_{T,0}$. The optimization problem is formulated as follows for the lane change scenario

$$\min f(x_{E,0}, x_{T,0}) = h(x_{T,0}) - x_{E,0}. \tag{4.37}$$

Here, function $h(x_{T,0})$ refers to a constant velocity model used to approximate the threat vehicle motion. For a velocity $v_T > 0$, the final position of the target is given by $h(x_{T,0}) = x_{T,f}$. The feasible set C consists of all points $x_{E,0}, x_{T,0} \in \mathcal{X}$ for which there is no collision detected, i.e all the points for which the generated trajectory avoids a collision with the detected stationary threat vehicle in lane. Figure 4.7 provides a visual representation of the bisection approach applied to lane change scenario.

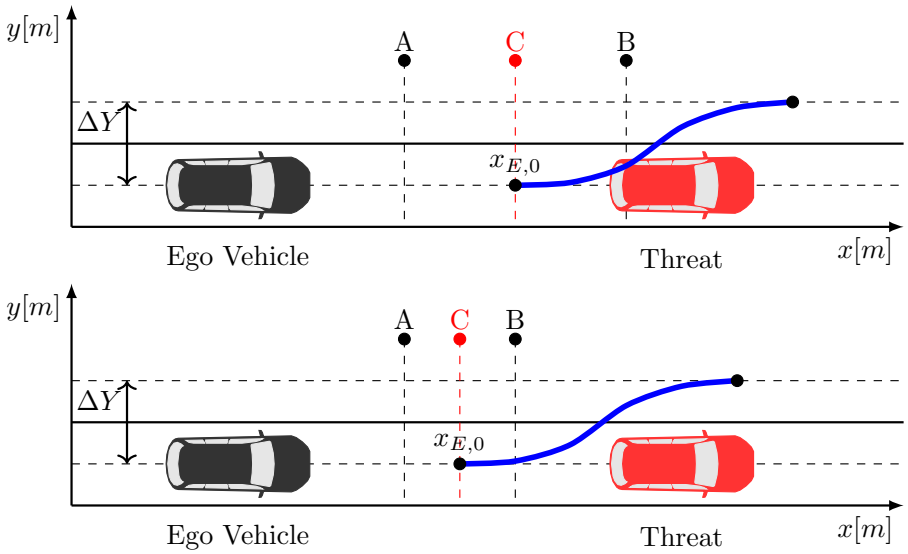

Figure 4.7: Bisection method to determine the last point to initiate lane change to avoid collision with threat vehicle.

4.3.3.2 Path Planning using Clothoid Curves

The path planner consists of a Bi-elementary path generator which is based on clothoids. The Bi-elementary path is built up of four clothoids of which the curvature is varying linearly with arc length.

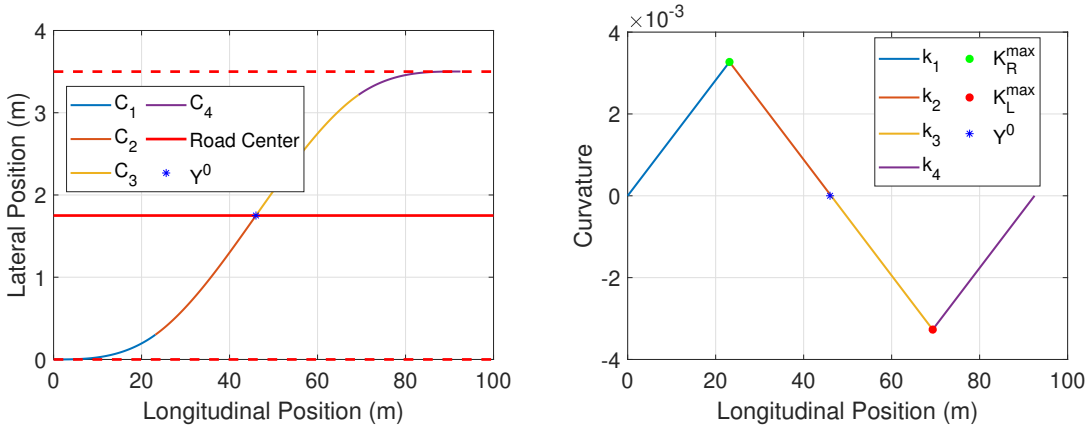

Figure 4.8: Bi-elementary lane change trajectory with maximum curvature defined by constant $\mu = 0.3$ and entry speed $30\frac{m}{s}$. Clothoids C_1 and C_2 make up an elementary path E_1.

Figure 4.8 shows the components of the Bi-elementary path along with the curvature over the arc length for a lane change trajectory under constant friction assumption. Clothoids are also known as Euler spirals or Cornu spirals and are defined as curves whose curvature varies linearly with the arc length $k(s) = \sigma s + k_0$. Here, σ is the rate of change of curvature or the sharpness [38]. The linear change in curvature is one of the reasons why clothoids are preferred in developing lane change trajectories for autonomous vehicles since it corresponds to constant angular velocity steering inputs.

The evolution of a clothoid depending on the arc length s is defined as:

$$\begin{aligned} \Psi(s) &= \Psi_0 + \int_0^s k(t)dt \\ X(s) &= X_0 + \int_0^s \cos(\Psi(t))dt \\ Y(s) &= Y_0 + \int_0^s \sin(\Psi(t))dt \end{aligned} \tag{4.38}$$

Here, X_0, Y_0, Ψ_0 are the initial position in global coordinates and the initial heading angle of the path and k is the curvature of the path. Figure 4.8 shows that the curve is symmetric about the center of the road. This is because of the constant road friction coefficient, which influences the maximum curvature to be equal on both lanes i.e $K_R^{max} = K_L^{max}$. The point Y^0, which is defined as the switch point, is the lateral position at which the curvature crosses the zero line as indicated in Figure 4.8. For constant friction scenarios, the switch point Y^0 is trivial as it is the lateral distance from start to the center of road.

The symmetry of the curve is disturbed when laterally varying friction profiles occur, which results in $K_R^{max} \neq K_L^{max}$ as shown in Figure 4.9. In such cases, if the position of the switch point is retained at the center of the road, it would result in a wider or narrower lane change trajectory depending on the friction profiles of each lane. Since the total width of the lane change ΔY is fixed, the optimal position of switch point Y^0 needs to be determined such that $\Delta Y_1 + \Delta Y_2 = \Delta Y$ holds. Here, ΔY_1 and ΔY_2 refers to the lateral displacement of each elementary path E_1 and E_2 as illustrated in Figure 4.9. The total lateral displacement of the lane change path is denoted $Y_f = \Delta Y_1 + \Delta Y_2$. The following section includes the description of the geometric approximation of Y^0 for a given clothoid path.

4.3.3.3 Computation of curve parameters for Bi-elementary path

This Section describes the computation of the curve parameters required to generate a lane change trajectory. The curve parameter include elementary path length S_2 and the switch point Y^0 which is a function of the elementary path length S_1. Using the change in curvature profile over time the resulting lane change trajectory is computed using 4.38 with the determined curve parameters.

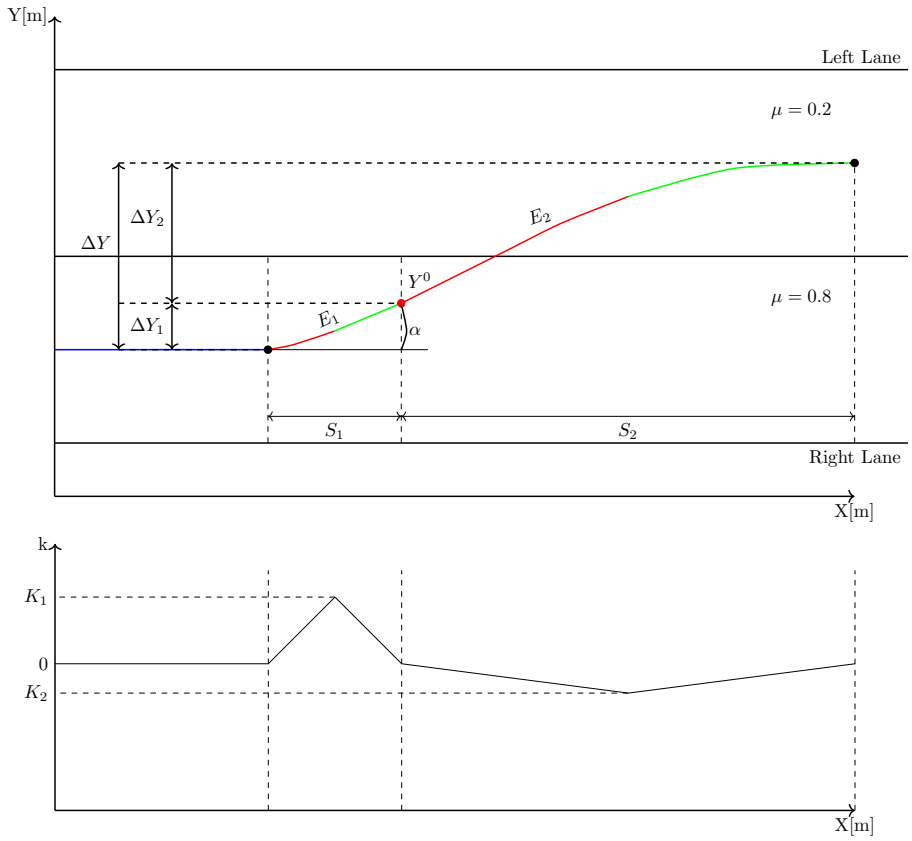

Figure 4.9: Visualization of components of Bi-elementary path for laterally varying friction profile.

Figure 4.9 illustrates the curve parameters that define the Bi-elementary path which consists of S_1, S_2 and Y^0. E_1 and E_2 are elementary paths each of which are made

up of two clothoids of equal length. This means elementary path E_1 is made up of C_1, C_2 and elementary path E_2 is made up of C_3, C_4. The length of each elementary part is defined as S_1, S_2. The maximum curvature of each elementary path depends on the road friction coefficient according to (4.35) so it can be represented as follows

$$\begin{aligned} K_1 &= K_R^{max} \\ K_2 &= K_L^{max}. \end{aligned} \tag{4.39}$$

Due to the varying maximum permissible curvature limits across the lanes, the resulting path is no longer symmetric about the road center. The resulting path planning problem boils down to determine curve parameters Y^0, S_1 and S_2 given an initial start point $x_{E,0} = (X_0, Y_0)$ and the maximum curvature at each lanes K_R^{max}, K_L^{max} such that $\Delta Y_1 + \Delta Y_2 = \Delta Y$ holds. An additional requirement in a lane change scenario, the heading at the start and the end of the lane change must be $\Psi_0 = \Psi_f = 0$ and this needs to be incorporated as a constraint on the path generation. Therefore, it must hold that

$$K_L^{max} = -\frac{K_R^{max} S_1}{S_2}. \tag{4.40}$$

The position of the switch point Y^0 is always equal to the lateral displacement of elementary path E_1 as illustrated in Figure 4.9.

$$Y^0 = \Delta Y_1. \tag{4.41}$$

From the introduced parameters of Bi-elementary paths and the constraints on orientations of the lane change path the final orientation of the elementary path E_1 is written in terms of length S_1 and maximum curvature K_R^{max} is determined from (4.38) to be:

$$\alpha = \frac{K_R^{max} S_1}{2} \tag{4.42}$$

And from [44] the change in length of an elementary part with respect to α is given as:

$$D(\alpha) = \int_0^{0.5} \cos(2\alpha(-t^2 + t))dt \tag{4.43}$$

Using Equations (4.42) and (4.43) the change in lateral position for the elementary path E_1 described in (4.41) is written as

$$\Delta Y_1 = S_1 \sin(\frac{\alpha}{2})\tilde{D}(\alpha), \tag{4.44}$$

where $\tilde{D}(\alpha)$ is a third degree polynomial approximation of the continuous function $D(\alpha)$ in (4.43). The coefficients for the polynomial were selected based on the work carried out in [39]. Using (4.40), (4.42) and (4.44) a bisection search method is applied to determine the optimal switch point Y^0 for which the resulting total path width $\Delta Y_f = \Delta Y$ the desired lane change width holds. The following section explains the algorithm used to determine the optimal switch point and the corresponding elementary path lengths S_1 and S_2 to obtain the desired lane change trajectory for laterally varying friction profiles.

4.3.3.4 Trajectory Planner Algorithm

Using the terms and relations introduced in the previous sections the lane change trajectory is computed which incorporates constraints on maximum permissible curvature. This section summarizes the trajectory planner algorithm developed to generate the lane change trajectory.

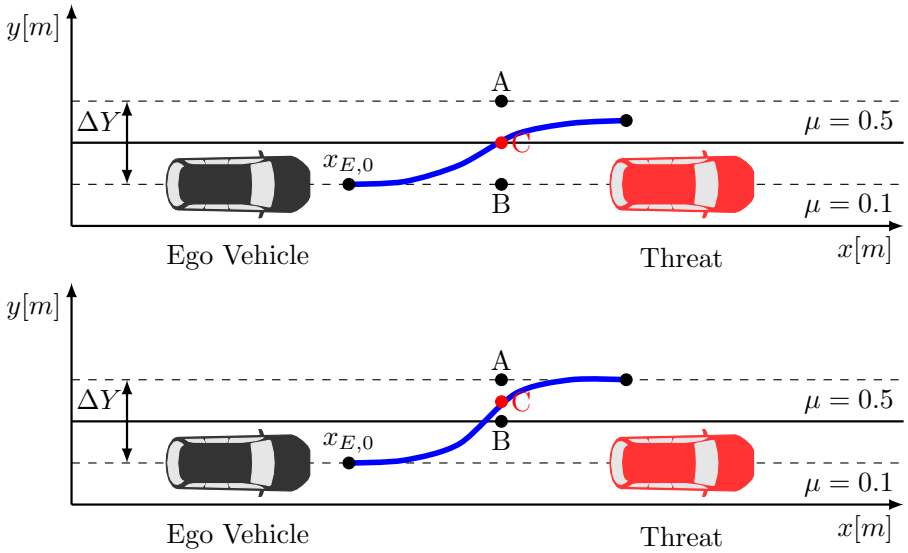

Figure 4.10: Visualization of Bisection Method applied to select the curvature switch point Y^0. Here point C refers to the candidate switch point Y_i^0

An initial candidate start point $x_{E,0}$ is chosen based on bisection method described in Section 4.3.3.1 and the maximum permissible curvatures at each lane K_R^{max} and K_L^{max} are computed using the friction information which is available. Upper and lower bounds of the switch point are defined based on the dimensions of the road

$$(A, B) = (Y_{max}^0, Y_{min}^0), \tag{4.45}$$

where Y_{max}^0 is the distance between both lane centers and Y_{min}^0 is zero(see Figure 4.10). The mid point of the interval between A and B is selected as the candidate switch point $C = Y_i^0$. Based on this candidate the lane change parameters S_1, and S_2 can be computed by solving (4.40), (4.42) and (4.44) with $\Delta Y_1 = Y_i^0$. The resulting Bi-elementary path is analyzed in terms of its final lateral displacement $Y_f = \Delta Y_1 + \Delta Y_2$. Depending on if the width is less or greater than the required lane change width $\Delta Y = 3.5$m, the interval A and B is adjusted and the trajectory is recomputed with a new candidate Y_i^0. When the algorithm converges to a solution the resulting lane change trajectory is handed over to the collision detection which is the next function block in Figure 4.6. Algorithm 2 is the pseudo code for the Trajectory Planner algorithm.

Algorithm 2 Trajectory Planner Algorithm

```
Set ΔY = 3.5m
A = 0
B = ΔY
while N ≤ N_max do
    Calculate middle point between A and B
    C = (A + B)/2
    Determine curve parameters S1, S2, from (4.44), (4.42), (4.40).
    Get trajectory from (4.38): [X Y Ψ]^T
    if Y_f − ΔY = 0 or (B - A) ≤ tolerance then
        Solution found and output trajectory [X Y Ψ]^T
    else
        N = N + 1
        if Y_f > ΔY then
            B = C
        else
            A = C
        end if
    end if
end while
```

4.3.3.5 Noisy friction measurements

This section describes the modifications made in the trajectory planner algorithm described in Section 4.3.3.4 to account for noisy measurements of predicted road friction information from the sensors. As presented in Section 4.3.3.3 the Bi-elementary path is generated based on the maximum curvature on each lane given the friction information. This means for each lane a friction value has to be known which can be incorporated as a constraint on the path's curvature. For noisy measurements, the friction in each grid cell (see Figure 2.1) is varying and the true friction of the lane is unknown. To account for this uncertainty and avoid overestimation of the available friction the assumed friction per lane is chosen in the following way.

By defining road patches for each lane the trajectory planner algorithm selects the minimum of the 3σ lower bound of all grid cells within the defined road patch for each lane. The first road patch is selected between the ego vehicle position at the start of the lane change $x_{E,0}$, and the threat vehicle $x_{T,0}$. The width of each road patch is equal to the width of the ego vehicle plus the distance to the road center lane. The minimum of the lower bound 3σ is selected from the patch to determine the maximum curvature K_R^{max} and the curve parameter S_1 is computed. Using the computed curve parameter S_1 the second road patch on the left lane is constructed at a distance S_1 from the ego vehicle up-to-the front bumper position of the threat vehicle. Once again, the minimum of the lower bound 3σ is selected from this patch to determine K_L^{max}. These defined limits for the curvature on the left and right lane can now be used in the algorithm defined in Section 4.3.3.4 to determine the full trajectory as part of the optimization loop.

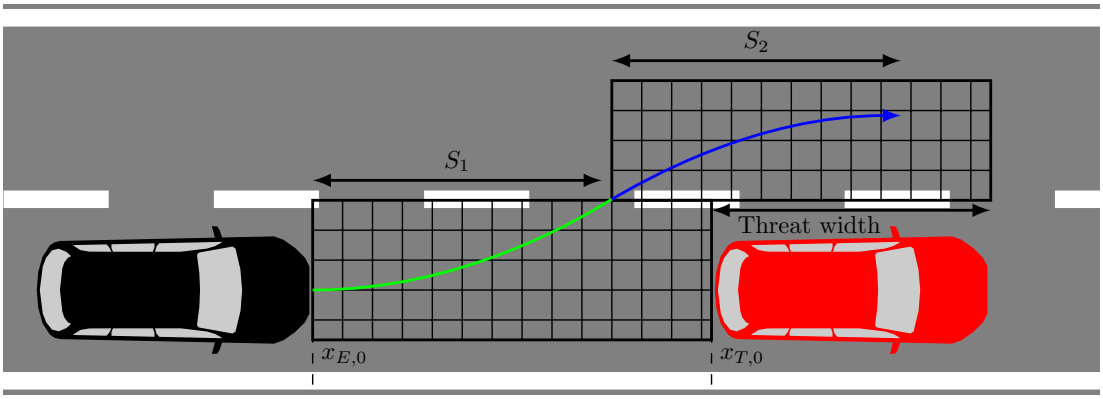

Figure 4.11: Visualization of road patches used to select friction coefficient of each lane in the presence of noisy measurements.

4.3.3.6 Collision Detection

For each generated lane change trajectory from the trajectory planner, collision detection is performed to evaluate the feasibility of the trajectory. This is done by defining the target vehicle as a polygon with specified added safety parameters in lateral and longitudinal directions. The approximation of the motion of the ego vehicle along the trajectory is performed using polygons that describe the actual vehicle dimensions. The polygons are evaluated to check if an overlap between the ego vehicle and the target vehicle occurs. If there is an overlap, the algorithm outputs a collision flag, the resulting start point $x_{E,0}$ is deemed unfeasible and the trajectory is discarded. A new trajectory is computed with a new start point selected by the optimization.

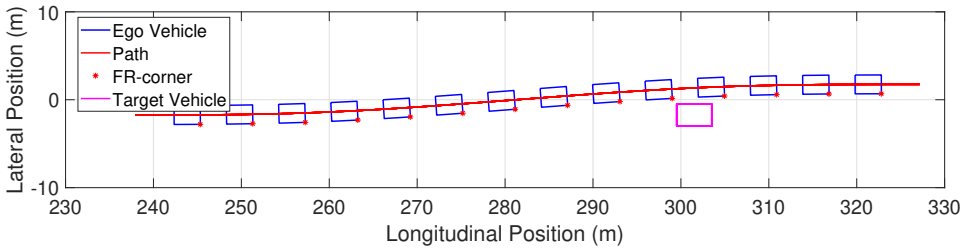

Figure 4.12: Collision Detection on Bi-elementary path

4.3.4 Decision Making for AES

A simple decision-making block is implemented in the AES architecture to determine the time at which the emergency lane change should be initiated. At each time step, the decision-making block evaluates the ego vehicle's current position with the start point of the trajectory that is computed by the trajectory generation block. If the current vehicle position is equal to the start point of the lane change, then the decision-making block switches signals to the controller to initiate the lane change maneuver. This is done by changing the reference signal to the control to be the lane change trajectory.

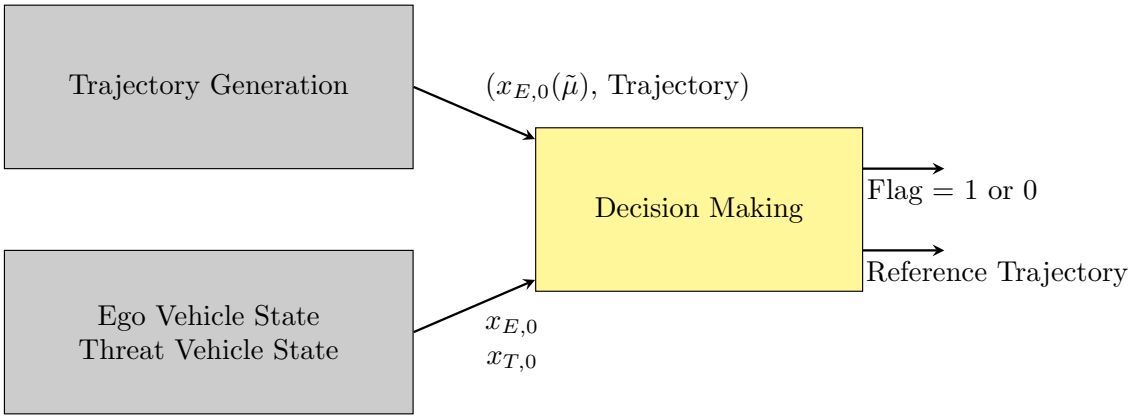

Figure 4.13: Decision Making block diagram

4.3.5 Path Tracking Controller

To ensure the ego vehicle tracks the computed lane change reference trajectory a lateral controller was implemented similar to the lateral controller used for the AEB scenario explained in Section 3.2.2 with some adjustments. Once the decision making triggers the flag to initiate a lane change maneuver, the lateral controller steers the vehicle along the computed reference trajectory. Using the steering angle as input $\delta(t)$, a lateral controller as proposed in [20] was implemented. The controller minimizes the lateral cross track error between the computed reference trajectory and the front axle position of the ego vehicle $e(t) = s_y^r(t) - s_y(t)$ and the error in heading $\Psi(t) - \Psi^r(t)$. In order to stabilize the yaw of the vehicle at high speeds an additional term is introduced in the control law, a negative feedback on the yaw rate $k_{dp}\dot{\Psi}(t) - \dot{\Psi}^r(t)$ that helps stabilize the yaw of the vehicle while minimizing the impact on tracking performance. The reference position $s_y^r(t)$ and orientation $\Psi^r(t)$ was the computed lane change trajectory from the trajectory generation block. The complete steering control law is defined as follows [20]:

$$\delta(t) = k_p(\Psi(t) - \Psi^r(t)) + arctan\frac{k_e e(t)}{k_{soft} + v(t)} + k_{dp}(\dot{\Psi}(t) - \dot{\Psi}^r(t)) \tag{4.46}$$

with $|\delta(t)| \leq \delta_{max}$, $v(t) \geq 0$ and $\frac{\pi}{6} \leq \delta_{max} \leq \frac{\pi}{6}$ is the maximum turn angle of the front wheels. The output from the lateral controller was multiplied with a steering ratio to convert to corresponding steering wheel angle which is used as lateral input in simulation environment CarMaker.

5
Results

In this chapter the results of the evaluation for the proposed AEB and AES algorithms are presented. All test results were achieved by simulation with the CarMaker simulation environment [5]. The simulated test vehicle is a Volvo XC90 with 4-Wheel drive and the vehicle parameters described in table 5.1.

Parameter name	Symbol	Value	Unit
Vehicle length	l_v	4.95	m
Wheel base	l	2.9840	m
Front axle to COG	a	1.4800	m
Rear axle to COG	b	1.5040	m
Mass	m	2078	kg
Width	w	1.664	m
Height of COG	h	0.73	m
Tire radius	r_w	0.3695	m

Table 5.1: Test vehicle parameters

5.1 Evaluation of AEB using road friction information

The proposed AEB algorithm is tested using different friction profiles and the vehicle behaviour is simulated (introduced in Section 5.1.1). The selected friction profiles help to study the influence of slippery patches of road segments on the AEB functionality. The system behaviour is evaluated assuming perfect predicted friction values as well as noisy predictions with zero-mean Gaussian noise and standard deviation of $\sigma = 0.1$. To assure that for noisy measurements the vehicle does not overestimate its braking performance the algorithm calculates the braking distance based on the 3σ lower bound of the distribution. As introduced in Section 1.3 the chosen evaluation metric is the distance to the threat vehicle at which the ego vehicle comes to standstill.

5.1.1 Friction profiles

The friction profiles are shown in Figure 5.1. The longitudinally varying friction profiles start 250m before the threat vehicle which is equal to the ego vehicle's radar range and therefore the first point at which the threat is detected. Before and after

the longitudinally varying patch the first and last friction value respectively is kept constant. The values vary discretely in steps of 0.1 from $\mu = 0.1$ to $\mu = 1$. When noise is added to the friction measurements also the noise is sampled from a discrete distribution resulting in discrete steps of 0.1.

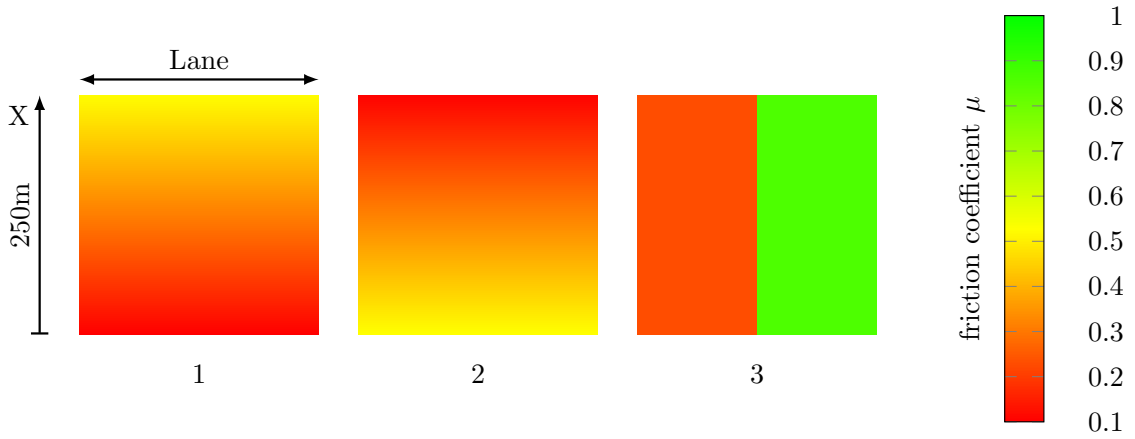

Figure 5.1: The evaluated AEB friction profiles: (1), (2) Longitudinal difference and (3) Lateral difference

5.1.2 Test scenario

We consider a rear end collision scenario, in which the ego-vehicle with a certain speed, is approaching a stationary threat vehicle. We assume the dynamic road friction profile ahead of the road is accessible to the ego vehicle. The goal is to determine the last point to initiate an AEB trigger given the road friction profile. The test track is a straight road without other obstacles. The threat vehicle is positioned in a distance of L offset in front of the ego vehicle (Figure 5.2). The initial distance is $L = 700$m and two velocity scenarios of $v_E = 30\frac{m}{s}$ and $v_E = 15\frac{m}{s}$ are tested.

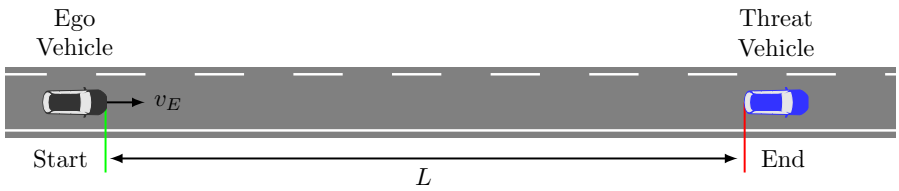

Figure 5.2: AEB scenario setup with ego vehicle starting in distance L behind threat vehicle.

5.1.3 Test results

The proposed algorithm achieves results of brake distance error in the range 0.5m to 5.5m on friction profiles 1 to 3 when accurate friction information is available. In comparison to the baseline systems assuming constant dry concrete the proposed algorithm improves the brake distance error 94.7% - 98.6% while preventing collisions in all test cases. In comparison to the baseline systems assuming constant snow the

proposed algorithm improves the brake distance error 87.7% - 98.1%. Table 5.2 shows the achieved results for the friction profiles.

Friction Profile	1		2		3	
Velocity [m/s]	15	30	15	30	15	30
Proposed [m]	0.5	0.8	1.4	5.5	0.9	2.8
Ass. dry [m]	-11.7	-42.6	-102.4	-384.6	-16.7	-58.8
Ass. snow [m]	11.5	24.8	-75.7	-131	7.3	36.9

Table 5.2: Error of Braking distance calculation in meters for different friction profiles for the proposed algorithm in comparison to assuming constant dry and snow road conditions

For noisy friction measurements the performance decreases as the algorithm's predictions become more conservative. This leads to large brake distance errors and potential false positives for AEB deployment (see Table 5.3). The results achieved

Friction Profile	1		2		3	
Velocity [m/s]	15	30	15	30	15	30
Mean [m]	37.8	68.1	71.5	131.6	13.9	56.3
Variance [m^2]	4.2	0	0	0	0.3	1.3

Table 5.3: Mean and Variance of the Error in Braking distance calculation in meters for different friction profiles assuming noisy measurements for 20 iterations.

from the proposed algorithm can be compared to [18], that utilizes a similar evaluation metric of error in brake distance estimations. The results achieved in [18] consider the ego vehicle to be travelling at a speed of 70kmph, with constant friction profiles ranging from $\mu = 0.3$ to 1. The absolute error in braking distance for those friction profiles are in the range of 0.005m to 0.01m. The work in [17] shows the AEB performance for high friction of $\mu = 0.85$ in terms of braking distance error. For the ideal case of perfectly known friction and ego vehicle speeds ranging from 40kmph to 80kmph the algorithm achieves an accuracy of 0.05m to 0.8m. While an assumption in [18] and [17] is that the friction stays constant along the prediction horizon, the proposed algorithm is able to prevent collisions for varying friction information.

5.2 Evaluation of AES using road friction information

Similarly to the AEB evaluation, the AES is evaluated using different friction profiles to study the influence of slippery patches of road segments on its functionality (see Section 5.2.1). Again the algorithms are tested assuming perfect measurements on the one hand and noisy measurements with zero-mean Gaussian noise and standard deviation of $\sigma = 0.1$ on the other hand. The developed implementations using model predictive control and curve-based path planning are evaluated and compared based

on a common performance measure. The evaluation metric is as described in Section 1.3 as the distance to the threat vehicle at which a lane change maneuver is initiated. Based on this metric the proposed AES systems are compared to a baseline system which assumes constant friction values. The baseline system is introduced in Section 2.3.

5.2.1 Friction profiles

The friction values vary in discrete steps of 0.1 from $\mu = 0.1$ to $\mu = 1$. Three profiles are evaluated as shown in Figure 5.3, a constant low friction case and two laterally varying profiles with different friction on the left and right lane. Profile 1 simulates snowy conditions with a constant value of $\mu = 0.3$. Profile 2 and 3 simulate the change from a dry asphalt lane with $\mu = 0.8$ onto an icy lane with $\mu = 0.2$ and the other way around. Grid size Δs of the friction grid is set to $\Delta s = 1m$.

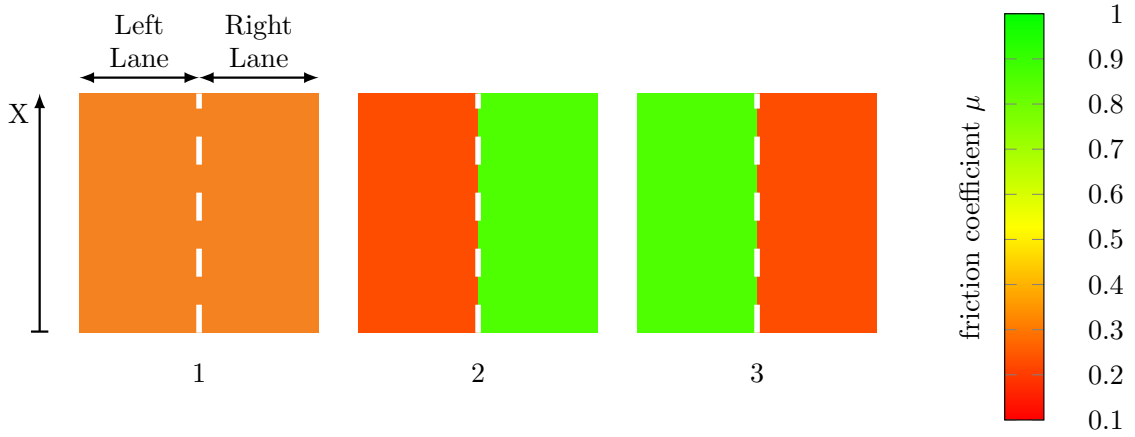

Figure 5.3: The evaluated AES friction profiles: (1) Low friction / snow, (2), (3) Different friction on left and right lane

5.2.2 Test scenario

The test case is a rear end collision scenario shown in Figure 5.4 with a stationary threat vehicle in distance L in from of the ego vehicle. The goal is to determine the last point at which an emergency lane change can be performed and execute the lane change before a collision occurs. The test track is a straight road with two lanes without any other obstacles. The initial distance is $L = 300$m for the scenario with ego vehicle velocity of $v_E = 30\frac{m}{s}$ and $L = 200$m for the scenario with ego vehicle velocity of $v_E = 15\frac{m}{s}$.

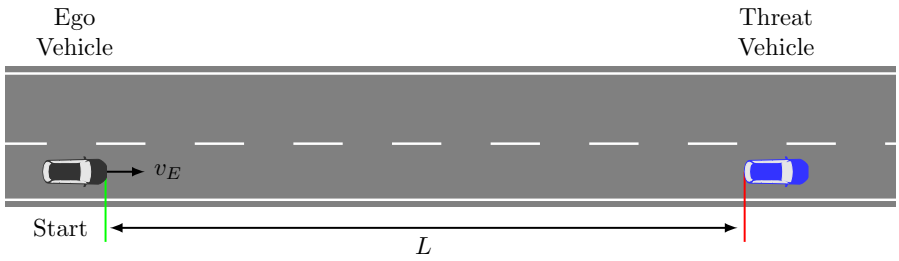

Figure 5.4: AES scenario setup with ego vehicle starting in distance L behind threat vehicle

5.2.3 Results of MPC based AES

The MPC vehicle model is based on the Volvo XC90 with parameters presented in Table 5.1. Further parameters used for the MPC vehicle model and optimization are listed in Table 5.4.

Parameter name	Symbol	Value	Unit
Ego vehicle chassis width	w_E	2.14	m
Ego vehicle chassis width	w_T	1.82	m
Front tire cornering stiffness	$C_{\alpha,f}$	45087	N/rad
Rear tire cornering stiffness	$C_{\alpha,r}$	44554	N/rad
Cost on lateral deviation to reference $\tilde{s}_y$	Q	10^8	
Cost on steering input	R	10	
Cost on steering rate	R_d	10^{10}	
Cost on slack variable ε	E	10^{10}	
Prediction Horizon	N	30	
System constraint maximum steering angle	δ^{max}	0.5	rad
System constraint minimum steering angle	δ^{min}	-0.5	rad
System constraint maximum steering rate	$\dot{\delta}^{max}$	0.1	rad
System constraint minimum steering rate	$\dot{\delta}^{min}$	-0.1	rad
System constraint maximum lateral acceleration	a_y^{max}	7	$\frac{m}{s^2}$
Safety distance in lateral direction	$s_{y,safety}$	0.2	m
Safety distance in longitudinal direction	$s_{x,safety}$	1	m

Table 5.4: MPC vehicle model and optimization parameters

We observe that for perfect measurements the MPC is able to prevent collisions in all cases and provide trajectories which make use of the dynamic friction information. Table 5.5 gives the achieved results for the MPC and the baseline system introduced in Section 2.3. The metric is the distance to the threat vehicle at which a lane change is initiated. A lane change initiation is assumed when the MPC applies a positive steering angle $\delta >= 5e^{-3}$. This way smaller lane keeping control actions shall be allowed without assuming the initiation of a lane change. It can be seen that the MPC determines varying points at which a lane change shall be initiated depending on the velocity and the friction profile, while the baseline systems give the same result independent of the friction. This leads for assumed constant dry concrete to

collisions in all test cases as the varying and low friction patches are not taken into account. This leads to a loss of control in the lane change maneuver and eventually to a collision with the threat vehicle or to sliding off the road. Assuming icy road conditions the baseline system behaves more conservatively and is able to prevent collisions in all cases, initiates the lane change earlier than necessary though. It can be seen that the MPC initiates the lane change later in all test cases and is still able to avoid collisions. This implies that the MPC is making better use of the available road friction.

Friction Profile	1		2		3	
Velocity [m/s]	15	30	15	30	15	30
MPC [m]	26.55	48.37	26.37	48.31	29.55	57.41
Ass. dry [m]	**19.00**	**34.36**	**19.00**	**34.36**	**19.00**	**34.36**
Ass. ice [m]	38.54	73.97	38.54	73.97	38.54	73.97

Table 5.5: Initiation of lane change relative to threat vehicle in meters for different friction profiles for the proposed MPC in comparison to assuming constant dry and icy road conditions. Collisions are indicated by bold, red numbers.

Figure 5.5 shows the resulting ego vehicle trajectories of the proposed MPC system for Friction Profile 1 (constant low friction) with ego vehicle velocity of $15\frac{m}{s}$ and $30\frac{m}{s}$. Clearly the obstacle is avoided and a smooth lane change is generated by the MPC regulator. It has to be noted that for Friction Profile 2 and 3 the MPC is not able to fulfill all given constraints at all times. These friction profiles impose a change in friction from the right to the left lane (see Figure 5.3).

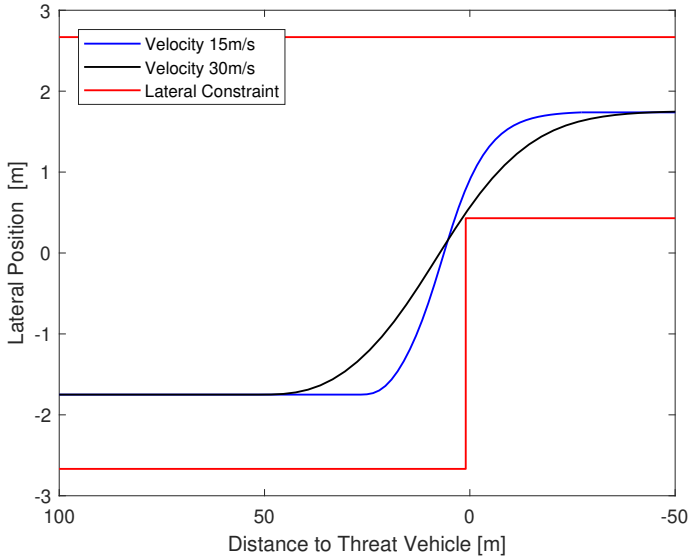

Figure 5.5: Friction profile 1, velocity $15\frac{m}{s}$ and velocity $30\frac{m}{s}$ with perfect measurements

The abrupt changes in constraints based on the friction profiles pose a challenge for the solver and lead to violations of the constraint set on the steering angle visualized

in Figure 4.3 at some time instances. This constraint is supposed to force the steering angle to $\delta \geq 0$ in the initiation of the lane change. The result is a trajectory which has a negative steering angle before the actual lane change is started. As shown in Figure 5.6 this is especially an issue for Friction Profile 2 where the change from a high to a low friction lane shows to be a challenge for the MPC system. It shall be noted though that even though the trajectory for Friction Profile 2 with velocity $30\frac{m}{s}$ violates the lateral constraint a collision is not occurring due to the safety distances that were added.

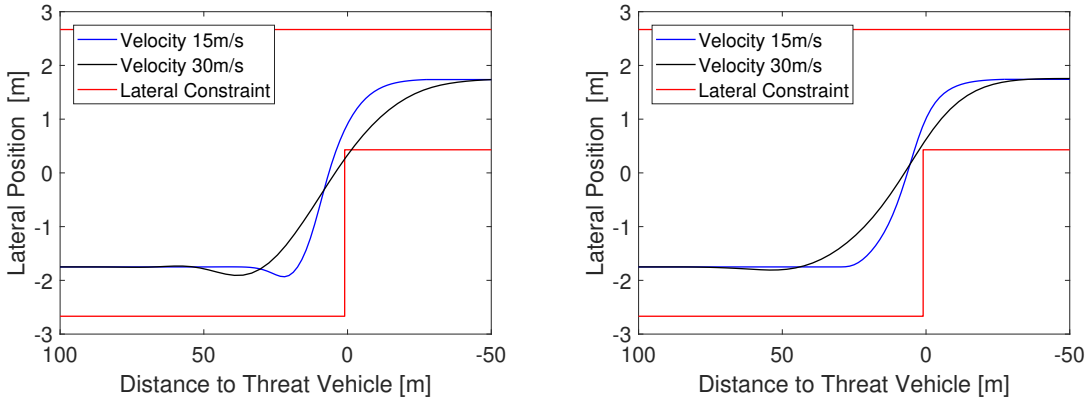

(a) Emergency lane change on friction profile 2

(b) Emergency lane change on friction profile 3

Figure 5.6: MPC trajectories for emergency lane change on friction profile 2 and 3 with perfect measurements

When noise is added to the measurements, similarly to the AEB function the 3σ lower bound of the distribution is calculated for each grid cell and handed over to the function. This shall lead to a rather conservative behaviour which ensures overestimation of the available friction is unlikely. Figure 5.7 shows the resulting trajectories for Friction Profile 1 (constant low friction) under the influence of noisy measurements for 20 simulation runs. It can be seen that rapid changes in road friction can be challenging for the MPC optimization. With added noise on friction values the constraints on the lateral forces at the tires are changing in each prediction step. This discontinuity causes problems to the solver and leads to convergence to infeasible points and therefore violations of the set constraints. Clearly the noise shows to have a big impact on the initiation of the lane change as well as the smoothness of the trajectory. While all collisions with the threat vehicle can be prevented for velocity $15\frac{m}{s}$, in multiple simulations the vehicle was not able to return back to a stable trajectory on the left lane and slid off the road. For the higher velocity case with $30\frac{m}{s}$ the trajectories showed more stability in terms of returning to the center of the lane, though two test runs resulted in collisions with the threat vehicle.

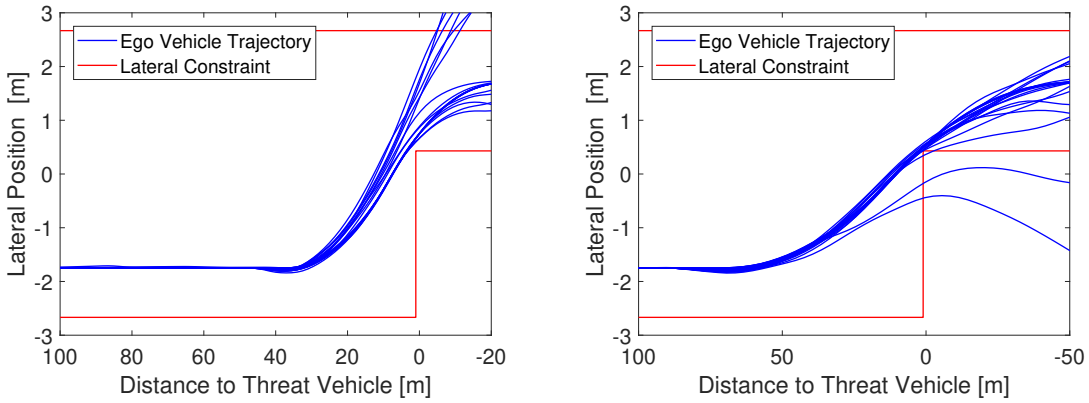

(a) Emergency lane change with a velocity of $15\frac{m}{s}$

(b) Emergency lane change with a velocity of $30\frac{m}{s}$

Figure 5.7: MPC trajectories for emergency lane change on friction profile 1 with noisy measurements including failed lane changes.

Simulations with noisy measurements for Friction Profile 2 and 3 show similar results with unstable trajectories. The full list of results can be seen in Table 5.6. On Friction Profile 2 the system already showed weaknesses for perfect measurements and was not able to give feasible results fulfilling all constraints. With noisy measurements collisions can only be prevented in few cases and the MPC has problems solving the objective function to a feasible solution.

Friction Profile	1		2		3	
Velocity [m/s]	15	30	15	30	15	30
Mean [m]	41.25	79.24	40.70	84.82	38.40	75.25
Variance [m^2]	2.24	28.44	27.82	24.14	0.92	18.44
Crashes	30%	10%	0%	80%	0%	10%

Table 5.6: Initiation of lane change relative to threat vehicle in meters for noisy friction. Crashes as percentage of simulation runs for which a collision occurred or the vehicle left the road due to loss of control.

5.2.4 Results of Path Planning based AES

The vehicle parameters used for simulation are found in Table 5.1. The lateral and longitudinal safety margins around the threat vehicles was selected to be equal to the safety parameters used in the MPC implementation to ensure the test settings are uniform across both platforms. Therefore, the lateral safety constraints used in the MPC was transformed to polygons around the threat vehicles as shown in Figure 5.8.

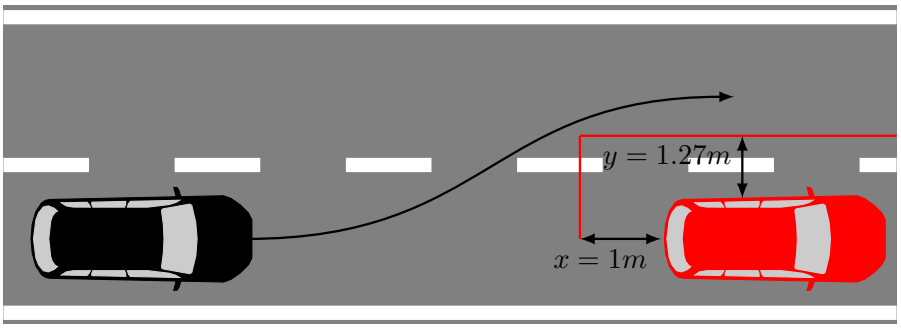

Figure 5.8: Lateral and longitudinal safety distances at threat vehicle for lane change using curve-based path planning.

The results obtained using a curve-based path planning approach considering friction information is shown in Table 5.7. The metric used to evaluate the developed algorithm is the distance between the ego vehicle and threat vehicle at which the lane change is initiated by the algorithm. Figures 5.9 and 5.10 shows the generated trajectory for Friction Profile 1 - 3, for two initial velocities of the ego vehicle of $15\frac{m}{s}$ and $30\frac{m}{s}$.

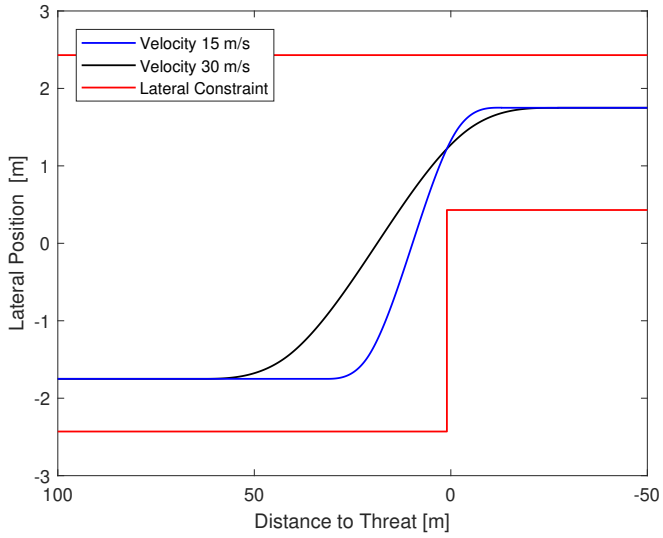

Figure 5.9: Friction profile 1, velocity $15\frac{m}{s}$ and velocity $30\frac{m}{s}$ with perfect measurements

We observe that for perfect measurements the emergency path planning algorithm is able to prevent a collision in all the test cases. The resulting trajectories generated from the clothoids are smooth and have curvature constraints incorporated in them that accounts for the varying friction profiles. Comparing the trajectories generated for Friction Profile 2 and 3, it can be seen that for Profile 2 the algorithm delays the lane change manoeuvre to make use of the high friction in right lane. In contrast, for Profile 3, since the friction is low the in the right lane, path planning algorithm initiates the lane change early. The tracking performance of the lateral controller implemented to follow the generated trajectory is illustrated in Figure 5.11.

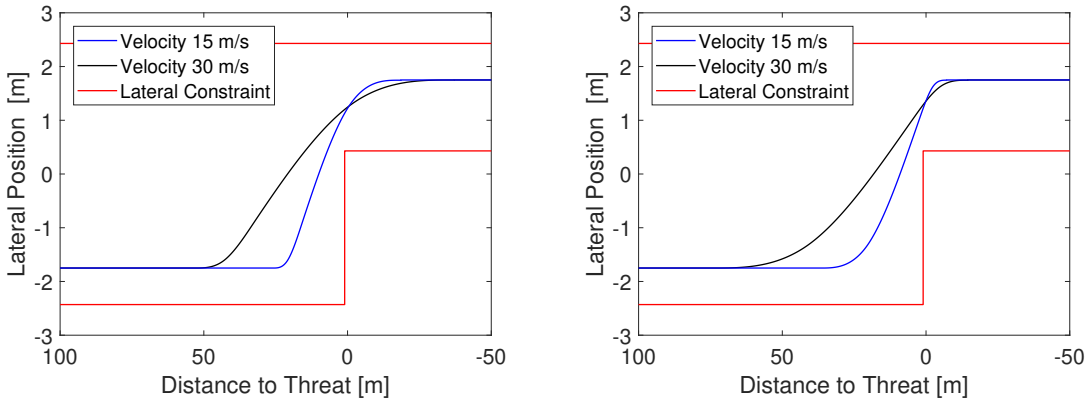

(a) Emergency lane change on Friction Profile 2

(b) Emergency lane change on Friction Profile 3

Figure 5.10: Path planning trajectories for emergency lane change on Friction Profile 2 and 3 with perfect measurements

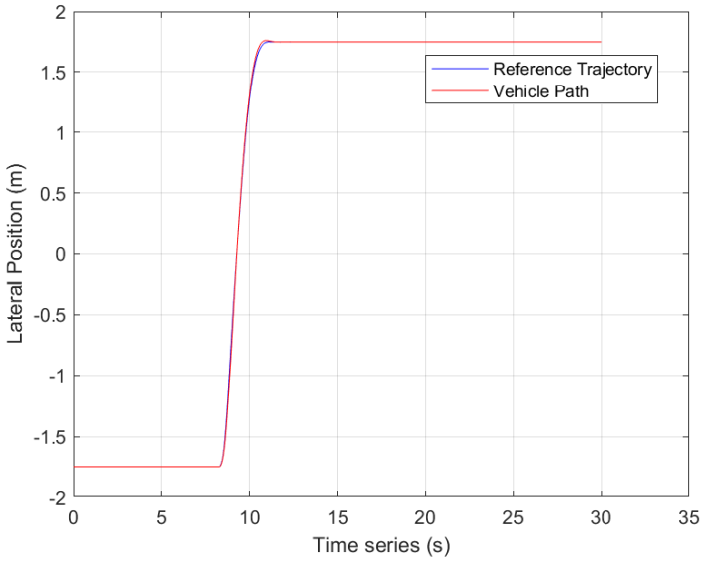

Figure 5.11: Lateral Controller Tracking for Friction Profile 2, velocity $30\frac{m}{s}$ with perfect measurements

It shows that the vehicle is able to closely track resulting trajectories generated using Bi-elementary clothoids. The resulting curvature profile of the generated trajectories ensures that the lateral forces acting on the tires of the vehicle do not lead to a tire saturation during the lane change manoeuvre. The algorithm was benchmarked against the path generation technique as described in Section 2.3 for two constant friction profiles, dry concrete and icy roads. The results obtained from the benchmark algorithm are explained in Section 5.2.3. Evaluation of path planning algorithm against the benchmarked algorithm showed similar results as the MPC, that the path planning algorithm was more efficient and managed to prevent collisions in all test cases.

Friction Profile	1		2		3	
Velocity [m/s]	15	30	15	30	15	30
Path Planning [m]	31.15	62.09	25.45	52.25	35.41	71.41
Ass. dry [m]	**19.00**	**34.36**	**19.00**	**34.36**	**19.00**	**34.36**
Ass. ice [m]	38.54	73.97	38.54	73.97	38.54	73.97

Table 5.7: Initiation of lane change relative to threat vehicle in meters for different friction profiles for the proposed Path Planning approach in comparison to assuming constant dry and icy road conditions. Collisions are indicated by bold, red numbers.

Also when considering noisy measurements of predicted friction information the path planning algorithm manages to avoid a collision in all the test scenarios. It shows though to be very conservative in its estimation of the last point to start a lane change to avoid overestimation of the available road friction. Figure 5.12 shows the generated trajectories for 20 simulation test runs with noisy measurements for Friction Profile 2. The resulting trajectories are smooth and consistent.

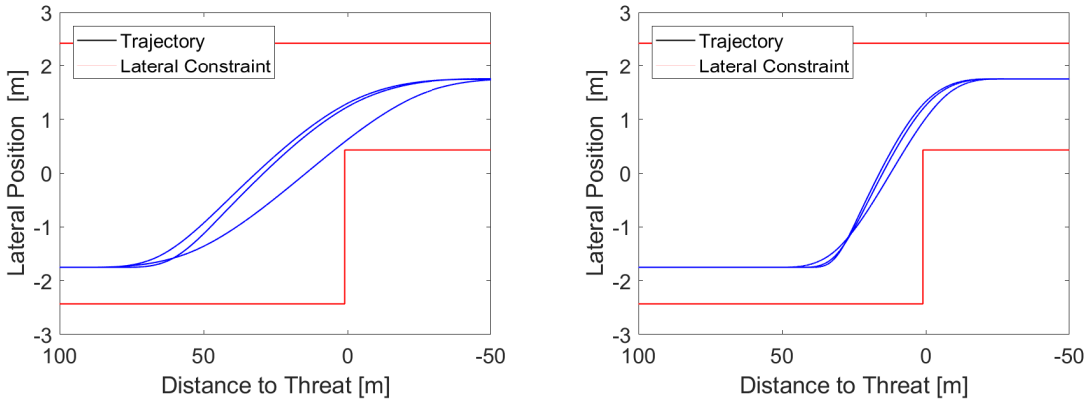

(a) Emergency lane change on Friction profile 2, $v = 30\frac{m}{s}$

(b) Emergency lane change on Friction profile 2, , $v = 15\frac{m}{s}$

Figure 5.12: Path planning trajectories for emergency lane change on Friction Profile 2 and 3 with noisy measurements

As it can be seen the algorithm converges to few trajectories, which results in a low variance in the lane change initiation. This is mainly due to the designed framework of the path planning algorithm and the selection of friction values for noisy measurements as explained earlier in Section 4.3.3.5. This is also the reason for the conservative behaviour of the algorithm which leads to early deployment of the maneuver but enables collision avoidance in all cases. The full list of simulation results for Friction Profiles 1 to 3 are shown in Table 5.8.

Friction Profile	1		2		3	
Velocity [m/s]	15	30	15	30	15	30
Mean [m]	49.5	89.2	41.3	86.55	49.55	89.13
Variance [m^2]	0	0	11.5	5.6	0	0
Collisions	0%	0%	0%	0%	0%	0%

Table 5.8: Initiation of lane change relative to threat vehicle in meters for noisy friction. Percentage of simulation runs for which a collision occurred or the vehicle left the road due to loss of control.

5.2.5 Comparison of MPC and Path Planning based Results

The proposed AES systems based on MPC and path planning approaches showed promising results in generating and tracking lane change trajectories to prevent collisions under dynamic friction conditions. Table 5.9 shows a compilation of the results achieved by MPC and Path Planner concerning the distance to the threat vehicle at which a lane change was initiated for perfect measurements. For most cases the MPC delivers a better result and is able to initiate the lane change later while still preventing a collision. This is mainly due to the framework of the MPC which performs optimization at each time step while the path planning algorithm on the other hand hits the maximum permissible curvature at just one point in space for each lanes. Friction Profile 2 proved to be a challenge for the MPC optimization which results in an unnecessarily early deployment and better results for the path planner.

Friction Profile	1		2		3	
Velocity [m/s]	15	30	15	30	15	30
MPC [m]	**26.55**	**48.37**	26.37	**48.31**	**29.55**	**57.41**
Path Planning [m]	31.15	62.09	**25.45**	52.25	35.41	71.41

Table 5.9: Comparison of test results for the proposed MPC and Path Planning based AES solutions. Best value per test case in green.

When noise is added to the measurements the MPC is in many cases unable to find feasible solutions which are not violating the constraints. This prevents successful collision avoidance in many cases. Table 5.10 shows the percentage of prevented collisions for the 20 simulation runs in each test case. Clearly the path planner is more robust against the added noise and keeps providing smooth lane change trajectories.

Friction Profile	1		2		3	
Velocity [m/s]	15	30	15	30	15	30
MPC [m]	70%	90%	100%	20%	100%	90%
Path Planning [m]	100%	100%	100%	100%	100%	100%

Table 5.10: Comparison of prevented collisions for test cases with added noise on measurements as percentage of run simulations.

6
Conclusion

In this thesis, two collision avoidance applications have been developed which utilize dynamic road friction information. Firstly an AEB system was proposed which makes predictions on the last possible point of braking based on an optimization problem. A simplified vehicle model has been developed which enables fast online computation and is used in the bisection method based optimization approach. Based on different experimental friction profiles it was shown that the proposed AEB algorithm is able to prevent collisions by braking for many dynamic friction profiles while also reducing the risk of false-positive interventions.

Secondly, two approaches for an AES system taking dynamic road friction into account have been developed. One approach is based on model predictive control and sets constraints on the vehicle dynamics based on the given friction profile. The second approach generates a trajectory with a maximum curvature defined by the given friction ahead of the vehicle. It is demonstrated that both approaches are able to prevent crashes in dynamic friction environments. While the MPC gives optimal results for perfect friction measurements it was shown that noisy measurements induce infeasibilities and lead to collisions in several cases. The path planning approach was shown to be more conservative but able to provide smooth and feasible trajectories in all test cases.

Bibliography

[1] P. A. Pisano, L. C. Goodwin, and M. A. Rossetti, "U.s. highway crashes in adverse road weather conditions," in *24th Conference on International Interactive Information and Processing Systems for Meteorology, Oceanography and Hydrology*, 2008.

[2] H. Brodsky and A. Hakkert, "Risk of a road accident in rainy weather," *Accident Analysis & Prevention*, vol. 20, no. 3, pp. 161–176, 1998.

[3] S. Roychowdhury, M. Zhao, A. Wallin, N. Ohlsson, and M. Jonasson, "Machine learning models for road surface and friction estimation using front-camera images," in *2018 International Joint Conference on Neural Networks (IJCNN)*, pp. 1–8, IEEE, 2018.

[4] Forensic Dynamics Inc., "Stopping (braking) distance calculator." Available: `http://forensicdynamics.com/stopping-braking-distance-calculator`. Accessed on: 2020-05-14 [Online].

[5] *CarMaker 7.14*, IPG Automotive GmbH. Available: `https://ipg-automotive.com/products-services/simulation-software/carmaker/`. Accessed on: 2020-05-10 [Online].

[6] R. Rajamani, *Vehicle dynamics and control*. Mechanical engineering series, Springer, 2. ed ed., 2012.

[7] S. Khaleghian, A. Emami, and S. Taheri, "A technical survey on tire-road friction estimation," *Friction*, vol. 5, no. 2, pp. 123–146, 2017.

[8] A. Boukerche and R. E. De Grande, "Vehicular cloud computing: Architectures, applications, and mobility," *Computer Networks*, vol. 135, pp. 171–189, Apr. 2018.

[9] D. Schramm, M. Hiller, and R. Bardini, *Vehicle Dynamics*. Springer Berlin Heidelberg, 2018.

[10] M. Althoff, M. Koschi, and S. Manzinger, "CommonRoad: Composable benchmarks for motion planning on roads," in *2017 IEEE Intelligent Vehicles Symposium (IV)*, pp. 719–726, IEEE, 2017.

[11] J. Nilsson, P. Falcone, M. Ali, and J. Sjöberg, "Receding horizon maneuver generation for automated highway driving," *Control Engineering Practice*, vol. 41, pp. 124–133, 2015.

[12] H. Ren, T. Shim, J. Ryu, and S. Chen, "Development of effective bicycle model for wide ranges of vehicle operations," in *SAE 2014 World Congress & Exhibition*, pp. 2014–01–0841, 2014.

[13] H. B. Pacejka and E. Bakker, "THE MAGIC FORMULA TYRE MODEL," *Vehicle System Dynamics*, vol. 21, pp. 1–18, 1992.

[14] J. Feng, J. Ruan, and Y. Li, "Study on intelligent vehicle lane change path planning and control simulation," in *2006 IEEE International Conference on Information Acquisition*, pp. 683–688.

[15] Y. Hwang and S. B. Choi, "Adaptive collision avoidance using road friction information," *IEEE Transactions on Intelligent Transportation Systems*, vol. 20, no. 1, pp. 348–361, 2019.

[16] Y.-L. Chen, K.-Y. Shen, and S.-C. Wang, "Forward collision warning system considering both time-to-collision and safety braking distance," in *2013 IEEE 8th Conference on Industrial Electronics and Applications (ICIEA)*, pp. 972–977, 2013. ISSN: 2158-2297.

[17] I.-C. Han, B.-C. Luan, and F.-C. Hsieh, "Development of autonomous emergency braking control system based on road friction," in *2014 IEEE International Conference on Automation Science and Engineering (CASE)*, pp. 933–937, 2014. ISSN: 2161-8089.

[18] H. Kim, K. Shin, I. Chang, and K. Huh, "Autonomous emergency braking considering road slope and friction coefficient," *International Journal of Automotive Technology*, vol. 19, no. 6, pp. 1013–1022, 2018.

[19] U. Kiencke and L. Nielsen, *Automotive Control Systems*. Berlin, Heidelberg: Springer Berlin Heidelberg, 2005.

[20] G. M. Hoffmann, C. J. Tomlin, M. Montemerlo, and S. Thrun, "Autonomous automobile trajectory tracking for off-road driving: Controller design, experimental validation and racing," in *2007 American Control Conference*, pp. 2296–2301, IEEE, 2007.

[21] Y. Chen, M. Das, and D. Bajpai, "Improving time-to-collision estimation by IMM based kalman filter," pp. 2009–01–0162, 2009.

[22] L. Cosic, M. Vranjes, V. Ilkic, and V. Mihic, "Time to collision estimation for vehicles coming from behind using in-vehicle camera," in *2019 Zooming Innovation in Consumer Technologies Conference (ZINC)*, pp. 109–112, IEEE, 2019.

[23] E. Coelingh, A. Eidehall, and M. Bengtsson, "Collision warning with full auto brake and pedestrian detection - a practical example of automatic emergency braking," in *13th International IEEE Conference on Intelligent Transportation Systems*, pp. 155–160, IEEE, 2010.

[24] B. Jacobson, *Vehicle Dynamics Compendium for Course MMF062*. Chalmers University of Technology, 2015.

[25] J. B. Rawlings and D. Q. Mayne, *Model predictive control: theory and design*. Nob Hill Pub, 2009. OCLC: ocn430536884.

[26] E. F. Camacho and C. Bordons Alba, *Model Predictive Control*. Springer London, Limited, 2013. OCLC: 1066179705.

[27] V. Turri, A. Carvalho, H. E. Tseng, K. H. Johansson, and F. Borrelli, "Linear model predictive control for lane keeping and obstacle avoidance on low curvature roads," in *16th International IEEE Conference on Intelligent Transportation Systems (ITSC 2013)*, pp. 378–383, IEEE, 2013.

[28] C. Huang, F. Naghdy, and H. Du, "Model predictive control-based lane change control system for an autonomous vehicle," in *2016 IEEE Region 10 Conference (TENCON)*, pp. 3349–3354, IEEE, 2016.

[29] P. Falcone, F. Borrelli, J. Asgari, H. E. Tseng, and D. Hrovat, "Predictive active steering control for autonomous vehicle systems," *IEEE Transactions on Control Systems Technology*, vol. 15, no. 3, pp. 566–580, 2007.

[30] C. E. Beal and J. C. Gerdes, "Model predictive control for vehicle stabilization at the limits of handling," *IEEE Transactions on Control Systems Technology*, vol. 21, no. 4, pp. 1258–1269, 2013.

[31] K. Berntorp, R. Quirynen, and S. Di Cairano, "Steering of autonomous vehicles based on friction-adaptive nonlinear model-predictive control," in *2019 American Control Conference (ACC)*, pp. 965–970, IEEE, 2019.

[32] J. V. Frasch, A. Gray, M. Zanon, H. J. Ferreau, S. Sager, F. Borrelli, and M. Diehl, "An auto-generated nonlinear MPC algorithm for real-time obstacle avoidance of ground vehicles," in *2013 European Control Conference (ECC)*, pp. 4136–4141, IEEE, 2013.

[33] M. Brännström, E. Coelingh, and J. Sjöberg, "Decision-making on when to brake and when to steer to avoid a collision," *International Journal of Vehicle Safety*, vol. 7, no. 1, p. 87, 2014.

[34] D. Dolgov, S. Thrun, M. Montemerlo, and J. Diebel, "Practical search techniques in path planning for autonomous driving," in *Proceedings of the First International Symposium on Search Techniques in Artificial Intelligence and Robotics (STAIR-08)*, (Chicago, USA), AAAI, June 2008.

[35] A. Gasparetto, P. Boscariol, A. Lanzutti, and R. Vidoni, "Path planning and trajectory planning algorithms: A general overview," in *Motion and Operation Planning of Robotic Systems* (G. Carbone and F. Gomez-Bravo, eds.), vol. 29, pp. 3–27, Springer International Publishing.

[36] D. Madås, M. Nosratinia, M. Keshavarz, P. Sundström, R. Philippsen, A. Eidehall, and K.-M. Dahlén, "On path planning methods for automotive collision avoidance," in *2013 IEEE Intelligent Vehicles Symposium (IV)*, pp. 931–937. ISSN: 1931-0587.

[37] J. Chen, P. Zhao, T. Mei, and H. Liang, "Lane change path planning based on piecewise bezier curve for autonomous vehicle," in *Proceedings of 2013 IEEE International Conference on Vehicular Electronics and Safety*, pp. 17–22, 2013.

[38] J. Funke and J. Christian Gerdes, "Simple clothoid lane change trajectories for automated vehicles incorporating friction constraints," *Journal of Dynamic Systems, Measurement, and Control*, vol. 138, no. 2, p. 021002, 2016.

[39] A. H. M. A. Kahya and K. W. Schmidt, "Clothoid-based lane change trajectory computation for self-driving vehicles," *Çankaya University Journal of Science and Engineering*, 2017.

[40] J.-w. Choi, R. Curry, and G. Elkaim, "Path Planning Based on Bézier Curve for Autonomous Ground Vehicles," in *Advances in Electrical and Electronics Engineering - IAENG Special Edition of the World Congress on Engineering and Computer Science 2008*, pp. 158–166, Oct. 2008. ISSN: null.

[41] F. Valero, F. Rubio, C. Llopis-Albert, and J. I. Cuadrado, "Influence of the friction coefficient on the trajectory performance for a car-like robot," *Mathematical Problems in Engineering*, vol. 2017, pp. 1–9, 2017.

[42] A. Mehmood, M. Liaquat, A. I. Bhatti, and E. Rasool, "Trajectory planning and control for lane-change of autonomous vehicle," in *2019 5th International*

Conference on Control, Automation and Robotics (ICCAR), pp. 331–335, 2019. ISSN: 2251-2446.

[43] M. Yue, X. Hou, X. Zhao, and X. Wu, "Robust tube-based model predictive control for lane change maneuver of tractor-trailer vehicles based on a polynomial trajectory," *IEEE Transactions on Systems, Man, and Cybernetics: Systems*, pp. 1–9, 2018.

[44] Y. J. Kanayama and B. I. Hartman, "Smooth local-path planning for autonomous vehicles1," vol. 16, no. 3, pp. 263–284. Publisher: SAGE Publications Ltd STM.